Published in final edited form as:
Nat Commun. ; 5: 3791. doi:10.1038/ncomms4791.

A population of glomerular glutamatergic neurons controls sensory information transfer in the mouse olfactory bulb

Roberta Tatti[1,2], **Khaleel Bhaukaurally**[#1,2], **Olivier Gschwend**[#1,2], **Rebecca P. Seal**[3], **Robert H. Edwards**[4], **Ivan Rodriguez**[2,5], and **Alan Carleton**[1,2]

[1]Department of Basic Neurosciences, School of Medicine, University of Geneva, 1 rue Michel-Servet, 1211, Geneva, Switzerland [2]Geneva Neuroscience Center, University of Geneva, Switzerland [3]Departments of Neurobiology and Otolaryngology, School of Medicine, University of Pittsburgh, 3501 Fifth Ave BST3 6058, Pittsburgh, Pennsylvania, 15260 [4]Department of Physiology and Neurology, School of Medicine, University of California, 600 16th Street, San Francisco, California 94143 [5]Department of Genetics and Evolution, University of Geneva, 30 quai Ernest-Ansermet, Geneva, Switzerland

[#] These authors contributed equally to this work.

Abstract

In sensory systems, peripheral organs convey sensory inputs to relay networks where information is shaped by local microcircuits before being transmitted to cortical areas. In the olfactory system, odorants evoke specific patterns of sensory neuron activity which are transmitted to output neurons in olfactory bulb glomeruli. How sensory information is transferred and shaped at this level remains still unclear. Here we employ mouse genetics, 2-photon microscopy, electrophysiology and optogenetics, to identify a novel population of glutamatergic neurons (VGLUT3$^+$) in the glomerular layer of the adult mouse olfactory bulb as well as several of their synaptic targets. Both peripheral and serotoninergic inputs control VGLUT3$^+$ neurons firing. Furthermore, we show that VGLUT3$^+$ neurons photostimulation *in vivo* strongly suppresses both spontaneous and odor-evoked firing of bulbar output neurons. In conclusion, we identify and characterize here a microcircuit controlling the transfer of sensory information at an early stage of the olfactory pathway.

Keywords

vesicular glutamate transporter; olfaction; external tufted cells; serotonin; channelrhodopsin

Correspondence should be addressed to A.C. (alan.carleton@unige.ch).

AUTHOR CONTRIBUTIONS: A.C., I.R., R.T., K.B. and O.G. carried out the study conceptualization and experimental design. R.T. performed immunohistochemistry and slice electrophysiology. K.B. performed calcium imaging experiments. O.G. performed *in vivo* electrophysiology experiments. R.S. and R.E. generated and provided Vglut3-cre mice. A.C. and R.T. wrote and edited the manuscript with comments from K.B., O.G., R.S., R.E. and I.R.

Competing interests: The authors declare that no competing interests exist.

Europe PMC Funders Author Manuscripts

INTRODUCTION

In mammals, olfactory sensory neurons (OSNs) project their axons in a receptor-specific manner onto olfactory bulb glomeruli[1, 2]. At this level, OSNs establish synaptic contacts with the apical dendrites of olfactory bulb (OB) output neurons and with different populations of juxtaglomerular (JG) cells. Olfactory information is then transferred to olfactory cortices through M/T cells' axonal projections. JG cells establish dendro-dendritic synapses with each other and with M/T cells. Among the various JG cells, a population of excitatory neurons called external tufted (ET) cells, may play a major role in modulating the input from OSNs to M/T cells[3-6]. The current model describes the transfer of olfactory information as a multistep excitation mechanism (i.e. feedforward excitation) in which the inputs to M/T cells is augmented by ET cells. ET cells in fact receive stronger OSN inputs than MCs and are thought to drive OB output neurons through direct glutamatergic synaptic transmission[3-6]. This feedforward pathway is thought to be extremely important since direct inputs from OSNs to M/T cells are often too weak to evoke action potentials[6]. For this reason ET cells may represent a critical node to transfer odorant information to cortical areas. Here, we aimed to obtain a molecular marker of ET cells involving vesicular glutamate transporters to study how odorant information is transferred in the OB *in vivo*.

Vesicular glutamate transporters (VGLUTs) are essential to fill glutamate into synaptic vesicles and are sufficient to confer the glutamatergic phenotype[7, 8]. In mammals, three transporters have been identified: VGLUT1 [also called SLC17A7[7, 8]], VGLUT2 [SLC17A6[9-12]] and VGLUT3 [SLC17A8[13-16]]. In the adult OB, M/T cells express VGLUT1 while VGLUT2 is strongly expressed by OSNs terminals[17-19]. In the glomerular layer (GL), unidentified JG cells express VGLUT2 and VGLUT3, some of them being putative ET cells[13, 19].

In this study, combining mouse genetics, immunohistochemistry and electrophysiology we describe a previously uncharacterized population of cells expressing VGLUT3. These neurons could be classified as ET cells from a morphological and electrophysiological point of view. However, using optogenetic circuit dissection, we show that VGLUT3 neurons have a different connectivity profile than previously described ET cells and that they differentially connect JG cells and output neurons. Finally, we show that channelrhodopsin stimulation of VGLUT3 neurons strongly suppresses both spontaneous and odor-evoked firing of OB output neurons *in vivo*. Our data strongly suggest that VGLUT3 neurons can modulate M/T cells firing and as a consequence control the transfer of olfactory information to olfactory cortices.

RESULTS

VGLUT3 is expressed by some juxtaglomerular neurons

To characterize VGLUT3 neurons of the main OB, we used Vglut3-TOM and Vglut3-ChR2 mice (see methods and Fig. 1a). In the OB of adult animals, reporter-expressing neurons were exclusively found in the glomerular layer[13, 19] (GL) and displayed the morphology of external tufted (ET) cells characterized by a pear-shaped soma and an apical dendrite ramifying a large portion of a single glomerulus (Fig. 1b-g). The labeling was local with no

sign of long-range centrifugal projections (Fig. 1b,c). VGLUT3 neurons often had axons ramifying into GL, external plexiform layer (EPL), internal plexiform layer and to a lesser extent to the granule cell layer (Fig. 1c,d).

To determine whether genetic labeling accurately reported endogenous expression of VGLUT3, we performed immunolabeling for VGLUT3 on slices from 8 week old Vglut3-TOM mice (Fig. 1h). All immunostained VGLUT3 cells were TOM^+ and ~95% of TOM^+ cells expressed VGLUT3 (95 ± 1.3%, Fig. 1i). The remaining fraction may represent either cells starting to express VGLUT3, lack of uniform penetration of the antibody, cells which transiently expressed VGLUT3 or a non-specific expression of the reporter.

In summary, Vglut3-reporter mice specifically label glutamatergic neurons in the GL having the morphology of putative ET cells.

Heterogeneity of the VGLUT3 population

To characterize the glutamatergic neurons located in the GL, we performed immunostaining for VGLUT1 and VGLUT2 on Vglut3-TOM slices from eight week old mice (Fig. 2a and Supplementary Fig. 1a-c). $VGLUT1^+$ and $VGLUT2^+$ cells were found in the GL though VGLUT1 expressing cells were more often located at the base of GL (i.e. border between GL and EPL). As the expression of VGLUTs may be developmentally regulated, we quantified the density of neurons expressing different VGLUTs in the GL at three postnatal ages (2, 4 and 8 weeks). For all ages, TOM^+ neurons were three to six times less numerous than VGLUT1 or VGLUT2 neurons (Fig. 2b-d). In addition, the number of TOM^+ cells increased with age (Fig. 2d). The average density of TOM^+ cells was comparable to the density of immunostained $VGLUT3^+$ neurons (average density at 8 weeks = 15.8 ± 0.3 × 10^3 mm^{-3} and 17.5 ± 0.8 × 10^3 mm^{-3} for $VGLUT3^+$ and TOM^+, respectively; unpaired t-test $P = 0.13$, $t(3) = 1.9$, $n = 4$ animals, Fig. 2d).

We then tested whether Vglut3-TOM neurons expressed additional vesicular transporters (Fig. 2e-g). Approximately 20% of TOM^+ neurons co-expressed VGLUT1 independently of age (Fig. 2h). In contrast, VGLUT2 co-expression was age-dependent, starting at ~60% of the TOM population at 2 weeks and decreasing to ~20% at 8 weeks (Fig. 2h). Surprisingly, ~30-40% of TOM^+ cells co-expressed the vesicular GABA transporter VGAT at all ages (Fig. 2g,h). Though some VGLUT3 neurons express additional vesicular transporters, these neurons represent a minor fraction (~5% at 8 week old age) of the entire $VGLUT1^+$, $VGLUT2^+$ or $VGAT^+$ populations (Fig. 2g-i).

The expression of different vesicular transporters with VGLUT3 may indicate the existence of different subpopulations of VGLUT3 neurons. To test this possibility, we measured the soma size and observed that different populations of glutamatergic neurons located in the GL could be distinguished. VGLUT1 neurons had larger somata (Fig. 3a-d) and may represent tufted cells (TCs)[18, 19]. In contrast, TOM^+ and $VGLUT2^+$ cells could not be easily distinguished from each other but had larger soma than GABAergic neurons identified by the expression of the vesicular GABA transporter (VGAT; Fig. 3a-d). Finally, $VGLUT1^+/TOM^+$, $VGLUT2^+/TOM^+$, $VGAT^+/TOM^+$ neurons could be distinguished by

their soma size and could therefore represent three different subpopulations of VGLUT3 neurons (Fig. 3e-h).

Our data suggest that a subpopulation of Vglut3-TOM neurons may not only be glutamatergic but may also have a GABAergic phenotype, as indicated by the expression of the vesicular GABA transporter. In agreement, some VGLUT3 neurons, but not VGLUT1 and VGLUT2 cells, expressed the GABA synthetizing enzyme GAD67 suggesting that co-expression of GABAergic markers is unique to the VGLUT3 population in the GL of the mouse olfactory bulb (Fig.4a-d). We then tested whether the GABAergic subpopulation of Vglut3-TOM neurons expressed known markers for GABAergic periglomerular cells, such as the Ca^{2+} binding proteins calretinin (CALR) and calbindin (CALB)[20] or the tyrosine hydroxylase enzyme (TH)[21]. TOM^+ neurons frequently expressed CALB but rarely CALR or TH (Fig. 5a-c). While most GABAergic Vglut3-TOM neurons expressed CALB (94 ± 2.9%, n = 4 mice), ~70% of the $VGLUT3^+/CALB^+$ neurons were found to be GAD67 positive (Fig. 5d), suggesting that some $CALB^+$ neurons are exclusively glutamatergic.

In summary, Vglut3-TOM cells represent a heterogeneous population of juxtaglomerular neurons co-expressing different glutamate and GABA vesicular transporters.

Electrophysiological properties of VGLUT3 neurons

Since VGLUT3 neurons had the morphology of putative ET cells, we tested whether they displayed the electrophysiological properties previously reported for such neurons: 1-low membrane resistance; 2-resting membrane potential around −50 mV; 3-presence of sag and rebound spiking in response to hyperpolarizing current injection reflecting the activation of a hyperpolarization-activated cation current (I*h*); and 4-spontaneous rhythmic activity persisting in presence of GABAergic and glutamatergic receptor antagonists[22, 23]. To account for the diversity of the VGLUT3 population we recorded a large number of cells with different soma sizes and location in the GL. All VGLUT3 neurons exhibited a unique apical dendrite arborizing a single glomerulus and axons running in the GL/EPL, sometimes reaching the GCL (Fig. 6a-e). In agreement with the diversity of ET cells previously reported[22-28], several cells had basal dendrites whereas other did not.

During whole cell recording, we injected hyperpolarizing steps of current while holding the membrane potential at ~−50 mV. All tested cells (n = 50) had sag blocked by the specific I*h* antagonist ZD7288 (Fig. 6f; ΔV = 16.1 ± 0.4 and 0.4 ± 0.2 mV for ACSF and 10 μM ZD7288 respectively, paired t-test P = 0.00013, $t(3)$ = 25.9, n = 4 cells in 4 slices from 2 mice) and rebound spiking (Fig 6f). Then we added to the artificial cerebro-spinal fluid (ACSF) GABA and glutamate receptor antagonists dl-APV, NBQX, SR-95531 (GBZ), CGP 35348 (referred as antagonist mix). All neurons displayed bursting or regular spiking depending on the imposed membrane potential (n = 15 neurons, Fig. 6g). VGLUT3 neurons burst frequency ranged from 0.35 to 6 Hz[22], with a mean of 1.8 ± 1.2 bursts/sec (n = 52). We concluded that VGLUT3 neurons were spontaneously active. However, to exclude potential alterations of the firing properties due to the whole cell configuration, we recorded another set of Vglut3-TOM neurons in cell-attached configuration (Fig. 6h). All recorded cells, displayed spontaneous firing persisting after addition of the antagonist mix (Figs.

6h,i). On average, the mean firing frequency increased following drug application suggesting that most cells were tonically inhibited (Fig. 6i).

Moreover, to confirm that VGLUT3/GABAergic neurons were sampled in our recordings, we crossed Vglut3-TOM mice with GAD67-GFP mice and recorded from GFP^+/TOM^+ neurons in presence of the antagonist mix. All GFP^+/TOM^+ cells exhibited similar electrophysiological characteristics (Fig. 6j-l) and displayed similar rhythmic activity (burst frequency 1.9 ± 0.2 Hz; n = 40 for Vglut3-TOM *vs.* 1.3 ± 0.2 Hz; n = 12 for Vglut3-TOM/GAD67-GFP; Mann-Whitney test, $Z(50)$= 1.3, P = 0.2). Taken together these data suggest that all VGLUT3 neurons, including VGLUT3/GABAergic cells, have similar electrophysiological properties.

Lastly, it has recently been shown that ET cells can be depolarized by serotonin (5-HT) through direct activation of 5-HT2A receptors[29]. In agreement with this, we found that application of 5-HT increased the spontaneous firing frequency of Vglut3-TOM neurons. The effect was reversed by bath application of the 5-HT2A receptor antagonist 4F-4PP (Fig. 6m,n). In another group of cells, we applied the 5-HT2A receptor agonist TCB-2, which increased the spontaneous firing rate in all tested cells (Fig. 6o).

In summary, despite the heterogeneity observed by immunohistochemistry, all VGLUT3 neurons share similar anatomical and electrophysiological features characterizing ET cells (i.e. morphology, spontaneous bursting activity, I*h* current, response to 5-HT), suggesting that VGLUT3 neurons are ET cells.

VGLUT3 neurons response to sensory inputs stimulation

ET cells receive monosynaptic inputs from OSNs[4, 5, 24]. We thus verified whether VGLUT3 neurons receive direct olfactory nerve (ON) inputs (Fig. 7a-d). Low electric stimulation intensity failed to evoke response while higher intensities evoked graded EPSPs and bursts of action potentials (Fig. 7a) often followed by long lasting depolarization (n = 8 out of 10 cells; Fig. 7b). The latency of ON-evoked EPSPs was short (Fig. 7e), similar to values reported for monosynaptic ON response in ET cells[4, 5, 24]. However, we aimed to confirm that the EPSP latency was compatible with a monosynaptic connection. First, we placed the stimulating electrode above a glomerulus adjacent to the recorded cell. The stimulation evoked IPSPs were blocked by NBQX and APV, demonstrating the polysynaptic nature of these connections (Fig. 7c). The latency of ON-evoked IPSPs was significantly longer than the ON-evoked EPSPs latency (Fig. 7e). Second, since D2 and $GABA_B$ receptors depress ON synaptic transmission[30-32], we recorded ON-evoked EPSPs and applied $GABA_B$ and D2 receptor agonists (baclofen and apomorphine, respectively; Fig. 7d). Though the EPSP amplitude decreased (n = 3, from 19 ± 2.2 mV to 5 ± 2.5 mV in control and drugs, respectively; paired t-test, $t(2)$ = 8.3, P = 0.014), the latency remained unaffected (Fig. 7e). Taken together these data suggest that VGLUT3 neurons receive monosynaptic excitatory inputs from the ON.

Presently, little is known about the *in vivo* response of ET cells to odorants. We thus crossed Vglut3-cre mice with a Cre-activated reporter line expressing the genetically encoded Ca^{2+} indicator GCaMP3 (Fig. 7f and Supplementary Fig. 2). We monitored fluorescence changes

in response to odor applications in individual neurons from awake head-restrained mice (Fig. 7g-i). Odorant applications evoked both increase and decrease in fluorescence (Fig. 7h,i). The decrease of fluorescence is consistent with a decrease of firing rate mediated by ON-evoked IPSPs (Fig. 7c). Depending on the odorant, some cells switched between excitation and inhibition (Fig. 7i and Supplementary Fig. 2). Furthermore, neurons projecting to the same glomerulus had the same odorant-response profile (Supplementary Fig. 2). The fraction of cells excited and inhibited varied across odorants (Fig. 7j). On average, odorants excited ~40% of the VGLUT3 cells and inhibited 10% of them (Fig. 7k).

In summary, VGLUT3 neurons receive direct ON inputs and their odor-evoked response is odorant-specific and tuned by GABAergic neurons.

VGLUT3 neurons contact different types of bulbar neurons

To identify neurons receiving synaptic inputs from VGLUT3 neurons, we used an optogenetic approach to probe connectivity between Vglut3-ChR2 cells (Supplementary Fig. 3a-c) and different populations of OB neurons. Since ET cells are known to directly excite output neurons in the OB[3-5], we performed whole cell recordings from these neurons while stimulating Vglut3-ChR2 cells (Figs. 8a-l). In some tufted cells (TC, $n = 6$), light-evoked EPSPs were recorded at different frequencies of stimulation (Fig. 8b). These excitatory connections were small (amplitude of the first EPSP = 251 ± 51 μV at 30 Hz light-stimulation) but reliable since each action potential of the train evoked an EPSP, suggesting a direct excitatory connection. Consistently, the latency was compatible with monosynaptic connection (Supplementary Fig. 4). In other tufted cells ($n = 2$), light stimulation evoked IPSPs only at high stimulation frequency which were blocked by NBQX/APV and characterized by longer latencies (Fig. 8c,l and Supplementary Fig. 4), suggesting a polysynaptic inhibitory connections. Surprisingly, no PSPs were ever recorded in mitral cellshaving intact primary and lateral dendrites at any tested stimulation frequencies, suggesting that VGLUT3 neurons are not the population of ET cells previously reported to excite mitral cells (Fig. 8d,k).

To determine whether other neuronal populations of the olfactory bulb would receive synaptic inputs from VGLUT3 neurons, we recorded from granule cells but never found responses following light stimulation at any of the tested frequencies (Fig. 8k). We also patched juxtaglomerular neurons ($n = 149$ neurons) including PG neurons, short-axon cells and neurons displaying an ET cell morphology but being VGLUT3$^-$. We never found excitatory connections. In contrast, we recorded $GABA_A$-mediated inhibitory connections that were mainly monosynaptic ($n = 15/18$ connections) since IPSPs were reliably evoked by each action potential at low frequencies and were not blocked by NBQX/APV ($n = 15$, Fig. 8f) or a gap junction blocker ($n = 3$, Supplementary Fig. 5). The peak amplitude of light-evoked IPSPs was larger at high frequencies (Figs. 8g,h) and the latency was also compatible with a monosynaptic connection (Supplementary Fig. 4). These results are consistent with the immunostaining results, which already suggested that a subpopulation of VGLUT3 neurons expressing GABAergic markers could release GABA (Figs. 2e, 4c, and 5d). Interestingly, all the juxtaglomerular neurons receiving direct inhibitory inputs had the morphology of ET cells, although they were VGLUT3$^-$ (Fig. 8e). Interestingly, these

VGLUT3^{-} cells also exhibited electrophysiological properties of ET cells: low input resistance (154 ± 22 MΩ), depolarized resting membrane potentials (−49.2 ± 1.3 mV), presence of a sag and rebound spiking after hyperpolarizing current injection (Fig. 8i) and spontaneous firing in ACSF. Besides VGLUT2 labeling confirmed their glutamatergic phenotype (*n* = 4; Fig 8j). To confirm that VGLUT2^{+}/VGLUT3^{-} neurons represent a separate population of ET cells, we recorded VGLUT3^{-} cells in the GL displaying spontaneous rhythmic activity in presence of GABAergic and glutamatergic receptors antagonists. These cells had the morphology and electrophysiological properties of ET cells (Supplementary Fig. 6a-b) and all expressed VGLUT2 (*n* = 7 cells, Supplementary Fig. 6c). Therefore VGLUT2 is a marker of a different population of ET cells being VGLUT3^{-}, presumably identifying the previously described ET cells[3-6].

Taken together, these data suggest that VGLUT3 neurons differentially connect with mitral and tufted cells. Excitatory connections were never found on mitral cells, but were found on tufted cells. In addition, VGLUT3 neurons directly inhibited a population of ET cells that are VGLUT2^{+} but VGLUT3^{-}. By inhibiting ET cells mediating the multistep excitation, VGLUT3 neurons may affect odor-evoked responses of M/T cells.

VGLUT3 neurons suppress the firing of output neurons *in vivo*

We next studied the functional impact of VGLUT3 neurons on the activity of M/T cells *in vivo*. We used optrodes to record M/T cells[33-35] from control (*i.e.* not expressing channelrhodopsin) and Vglut3-ChR2 mice while stimulating the GL with blue laser (Fig. 9a,b). Photostimulation consistently reduced both spontaneous and odor evoked firing in M/T cells recorded specifically from Vglut3-ChR2 mice (Fig. 9c-e). At a population level, a large fraction of M/T neurons were inhibited in Vglut3-ChR2 mice (Fig. 9f-h). In modulated neurons, the inhibition was strong for both spontaneous and odor-evoked firing (average reduction: 75.7 ± 9% and 61.6 ± 3.4% for spontaneous and odor, respectively) and independent on the basal firing rate (Fig 9f,g). Notably, all cells modulated by photostimulation during odor application were also modulated during spontaneous activity (Fig. 9i). Finally, the light-evoked suppression of odor-evoked firing was observed in neurons either excited or inhibited by odorants (Fig. 9j).

In summary, these data suggest that VGLUT3 neurons can efficiently suppress both basal and odor-evoked firing of M/T cells. In conclusion, by controlling output neurons of the olfactory bulb, we propose that VGLUT3 neurons reduce the transfer of odorant information to cortical networks.

DISCUSSION

Here we report a previously uncharacterized population of glutamatergic neurons expressing VGLUT3 in the OB (Figs 1-5). Using optogenetics, we identified bulbar synaptic targets of VGLUT3 neurons (Fig. 8) and showed that stimulation of VGLUT3 neurons control the transfer of sensory information to cortical structures by suppressing both spontaneous and odor-evoked firing of output neurons (Fig. 9).

We used a genetic labeling approach to study the morphological and electrophysiological properties of VGLUT3 expressing neurons in the GL of the mouse OB. Almost all labeled cells in Vglut3-TOM mice expressed VGLUT3 protein suggesting that Vglut3-TOM mice reliably reveal the entire population of VGLUT3$^+$ neurons in the GL (Fig. 1). As reported in several brains regions[36-38], the expression of VGLUTs in the GL of the OB is developmentally regulated [Fig. 2; [18]]. From our study it emerges that VGLUT3 neurons represent the smallest population of glutamatergic cells in the GL, but its density increases with age. Additional work is required to investigate whether the observed increase in density reflects a switch in VGLUTs expression or an addition of adult-born neurons[39-42].

Our immunohistochemical characterization suggests that three subpopulations of VGLUT3 neurons can be identified by different markers and soma size: VGLUT1$^+$/VGLUT3$^+$, VGLUT2$^+$/VGLUT3$^+$ and VGAT$^+$/VGLUT3$^+$ (Fig. 2, 3, 4 and 5). It follows that VGLUT3 neurons can represent three separated subpopulations rather than a single population displaying developmental switching in vesicular transporter expression. In summary, sixty percent of VGLUT3$^+$ cells are purely glutamatergic (either VGLUT1$^+$/TOM$^+$ or VGLUT2$^+$/TOM$^+$) while the remaining VGLUT3 neurons also have a GABAergic phenotype (Figs. 2, 4, 5).

The existence of neurons showing both GABAergic and glutamatergic phenotype, though intriguing, is no longer new. In fact, the three VGLUTs can be expressed by non-glutamatergic neurons such as cholinergic, dopaminergic, noradrenergic, serotoninergic and GABAergic cells (see for review[43]). In particular, VGLUT3 is expressed by cholinergic neurons in the striatum and GABAergic interneurons in the cortex and hippocampus[13, 14, 44-47]. Co-expression of two vesicular transporters could be used by neurons to co-release neurotransmitters either at the same terminal or at different terminals (see for review [43]). If expressed on the same vesicle, a synergistic effect may also occur. In this last case, the addition of a vesicular transporter would increase the concentration of the primary neurotransmitter inside synaptic vesicles (see for review [43]). Future experiments will be needed to determine the precise location of different vesicular transporters within VGLUT3 neurons and the functional relevance of vesicular transporter co-expression.

Many authors have described ET cells morphology, basic electrophysiological properties and response to peripheral as well as top-down inputs[22-28]. The combination of morphological and electrophysiological features uniquely characterizing ET cells was observed for all VGLUT3 neurons, including the GABAergic/VGLUT3 subpopulation. We therefore claim that VGLUT3 neurons are undistinguishable from ET cells. However, the difference between VGLUT3 neurons and formerly identified ET cells relies on their synaptic targets. In the current circuitry model (Fig. 10a), though M/T cells receive monosynaptic inputs from OSNs[3-6], the excitation may not be sufficient to trigger action potentials[6]. A feedforward (otherwise called multistep) excitatory pathway mediated by ET cells which release glutamate on output neurons is supposed to amplify ON inputs. This mechanism is considered to be particularly important for MCs that receive weaker ON inputs than TCs. By using optogenetics, we found VGLUT3$^+$ neurons exclusively excite TCs but never mitral cells (Fig. 8). This result is not due to inaccurate sampling since we verified that MCs and TCs had intact apical dendrites. Furthermore, we obtained similar

results when performing pair recordings of MCs and VGLUT3-TOM neurons (more than one hundred pairs were tested and no connections were found). Thus our data indicate that VGLUT3 neurons do not correspond to the population of ET cell previously reported to excite mitral cells[3-6]. However, we identified another population of cells being $VGLUT2^{+}$ but $VGLUT3^{-}$ which also displayed morphological and electrophysiological features of ET cells (Fig. 8 and Supplementary Fig. 6). $VGLUT2^{+}/VGLUT3^{-}$ neurons may correspond to the ET cells previously described to excite MCs and mediate the feedforward excitation. Finally, we report a novel subpopulation of $ET^{VGLUT3+}$ cells directly inhibiting $ET^{VGLUT2+/VGLUT3-}$ cells.

What percentage of external tufted cells do VGLUT3 neurons represent? If we assume that VGLUT2 is the exclusive marker of external tufted cells, based on our data reported in Figure 2d, we can propose that ET^{VGLUT3} are three times less numerous that ET^{VGLUT2}. However, there are now evidences that uncharacterized glutamatergic neurons of the GL, which are not ET cells since they display dendrites and axons surrounding the glomeruli[39-42], also express VGLUT2. Therefore the relative fraction of VGLUT3 neurons to the total ET population may be higher than 25%.

Taken together, our data suggest that several populations of ET cells are present in the GL and we propose a novel model taking into account this diversity (Fig. 10b). In our model, $ET^{VGLUT2+/VGLUT3-}$ neurons would mediate the previously reported feedforward excitation on MCs and TCs. Furthermore, $ET^{VGLUT3+}$ cells inhibit $ET^{VGLUT2+/VGLUT3-}$ neurons thus reducing the input strength received by M/T cells and consequently their firing rate. Since $ET^{VGLUT3+}$ cells also excite tufted cells which also receive stronger nerve inputs than MCs[6], we can speculate that inhibition of the feedforward excitation mediated by $ET^{VGLUT2+/VGLUT3-}$ would affect more MCs than TCs. From our model, VGLUT3 neurons mediate both excitation on TCs and inhibition on $ET^{VGLUT2+}$. However, we cannot say whether different subpopulations (i.e. VGLUT3/GABAergic *vs.* VGLUT3/purely glutamatergic) would contact $ET^{VGLUT2+}$ and TCs or if the same subpopulation (i.e. VGLUT3/GABAergic) mediates both effects (Fig. 10a-c). In addition, stimulation of VGLUT3 cells evoked polysynaptic inhibition on TCs and on $ET^{VGLUT2+/VGLUT3-}$. We have not yet been able to identify the GABAergic interneurons excited by VGLUT3 neurons that are responsible for this polysynaptic inhibition since granule and periglomerular cells failed to show light-evoked excitation. However, given that each of these interneuron populations is thought to be extremely heterogeneous, we cannot rule out that subpopulations of granule or periglomerular cells, not sampled in our recordings, would receive direct excitation from VGLUT3 neurons. Furthermore, short-axons cells or parvalbumin interneurons in the external plexiform layer[48, 49], which were not sampled in our recordings, may account for the polysynaptic inhibition. Future studies will be needed to characterize the connectivity of specific VGLUT3 subpopulations as well as the precise origin of the synaptic contacts onto targeted neurons (axonal vs. dendritic).

Our *in vitro* data suggested that VGLUT3 neurons might control M/T cells firing. In agreement, VGLUT3 neuron stimulation strongly suppresses both spontaneous and odor-evoked firing in a large fraction of M/T cells *in vivo*, though some cells were unaffected (Figs. 8 and 9c). This non-homogenous effect is likely to be due to the local nature of the

photostimulation when using optrodes. However, weakly modulated neurons may also represent heterogeneity of response in the M/T cell population. Based on our *in vitro* data, we can speculate that MCs and TCs may be differentially modulated *in vivo*. MCs discharge following sensory inputs stimulation is more dependent on multistep excitation than tufted cells[6]. Therefore inhibition of $ET^{VGLUT2+}$ by $ET^{VGLUT3+}$ could have a more prominent impact on MCs than on TCs. Given that MCs and TCs are not discharging in the same phase in the respiratory cycle[50] and that they project to different cortical structures[51], modulation by VGLUT3 neurons could differentially control the two output pathways of the olfactory bulb.

By controlling olfactory bulb output neurons VGLUT3 cells contribute to control the transfer of information from sensory neurons to cortical centers and therefore participate in filtering out odorant information. But how are VGLUT3 cells going to be activated? A first way to recruit VGLUT3 neurons would be through direct synaptic inputs coming from OSNs. VGLUT3 neurons are also strongly inhibited either spontaneously or when the olfactory nerve is stimulated. Combination of excitation and inhibition will lead to complex odorant-specific recruitment of VGLUT3 neurons, as observed in calcium imaging experiments (Fig.7). A second way to activate VGLUT3 neurons would be through activation of serotoninergic afferents. We show that VGLUT3 neurons can be depolarized by 5-HT through activation of 5-HT2A receptors. Excitation of all VGLUT3 neurons through 5HT-2A receptors would be part of a general mechanism of control of input/output gain mediated by 5-HT, decreasing the release of glutamate by sensory neurons[52] and weakening the feedforward excitation pathway.

In conclusion, we propose that VGLUT3 neurons represent a novel population of bulbar neurons ideally positioned to control the transfer of odorant information from sensory neurons to cortex while being under the control of both bottom-up and top-down inputs.

METHODS

Animals

$Tg(Slc17a8\text{-}icre)^{1Edw}$ mice [referred as Vglut3-cre mice in the text, [53]] were crossed with three different Cre-activated reporter lines conditionally expressing either tdTomato[54], Channelrhodopsin2-YFP[55] or GCaMP3[56]. We analyzed the progeny derived from these crossings carrying the Cre driver and one reporter allele (referred as Vglut3-TOM, Vglut3-ChR2 and Vglut3-GCaMP3 mice in the text). In few experiments, Vglut3-cre::Rosa-floxStopflox-tdTom mice were crossed with GAD67-GFP knock-in mouse $Gad1^{tm1Tama}$ [57]. C57BL/6J mice were also used for data presented in Figure 4 and Figure 9. None of the experiments were performed blind of the genotype. Animals used for the experiments were coming from different litters. Both genders have been used throughout the study. Mice age is reported in other method sections or in figure legends.

All animal protocols are in accordance with the Swiss Federal Act on Animal Protection, Swiss Animal Protection Ordinance, and were approved by the University of Geneva and Geneva state ethics committees (authorizations 1007/3387/2 and 1007/3758/2).

Immunohistochemistry

Animals of different ages (see below and results) were deeply anaesthetized with an intraperitoneal injection of urethane 20% in 0.9% NaCl and perfused transcardially with 40 ml of saline followed by 50 ml of 4% paraformaldehyde (PFA) in 0.1M phosphate buffer at 4°C (PBS, pH 7.3). The brains were then dissected out and postfixed overnight in 4% PFA. After embedding brains in 4% agarose, forty micrometers slices (either coronal or horizontal) were cut with a vibratome (Leica VT S1000) and collected in PBS (0.1 M).

To stain YFP^+ neurons, we first blocked endogenous peroxidases by incubating the sections for 20 minutes with 0.7% H_2O_2 in TBSTT (Tris-buffered saline with tween and triton). After rinsing, they were blocked with 10% normal goat serum for 1 h at room temperature and then incubated with rabbit anti-GFP antibody overnight at 4°C (1:1000, Invitrogen). The day after, slices were rinsed and incubated with biotinylated goat anti-rabbit IgG (1:200, Invitrogen, catalog number A11122) for 1h at room temperature. Sections were then processed using avidin-biotin-peroxidase complex (ABC kit, Vectors laboratories) and reacted with the chromogen 3,3′ diaminobenzidine (DAB, Sigma Aldrich). Sections were mounted with DePeX mounting medium (Gurr).

For the age-dependent expression analysis, we used two, four and eight weeks old Vglut3-Tom mice (n = 4 animals in each group). For each staining, at least 100 cells (imaged from ~40 stacks taken from ~6 different slices) were analyzed per animal. Slices were incubated with one or two primary antibodies overnight, followed by appropriate secondary antibodies. Primary antibodies used were: rabbit anti-VGLUT1 (1:2000, Synaptic systems, cat. num. 13530); rabbit anti-VGLUT2 (1:1000, Synaptic systems, cat. num. 135403), rabbit anti-VGLUT3 (1:1000, Synaptic systems, cat. num. 135203); rabbit anti-VGAT (1:400, Synaptic systems, cat. num. 131003); mouse anti-GAD67 (1:1000, Millipore; cat. num. MAB5406), rabbit anti-Calretinin (1:1000, Swant, cat. num. 7699/4); rabbit anti-Calbindin (1:500, Swant, cat. num. 300); mouse anti-TH (1:500, Chemicon, cat. num. MAB5280). Secondary antibodies used were: Alexa 488 anti-rabbit (Invitrogen, cat. num. A21206), Alexa 546 anti-mouse (Invitrogen, cat. num. A21123), Alexa 647 anti-mouse (Invitrogen, cat. num. A31571). All secondary antibodies were diluted 1:200. Slices were counterstained with Hoechst (1:5000, Invitrogen, cat. num. H3570) and mounted with Vectashield (Vectors Laboratories). Images were acquired with a confocal laser-scanning microscope (Zeiss LSM 700) with 63× oil-immersion objective. Fluorescent channels were acquired in sequence to separate wavelength and minimize possible cross-talk. Projection images were made in ImageJ. Quantification of co-localization was done with the Zeiss LSM browser.

Slice electrophysiology

Experiments were performed on 6 to 8 weeks old *Vglut3*-Tom or *Vglut3*-ChR2 mice. Animals were anesthetized by isoflurane inhalation before decapitation. Olfactory bulbs extraction and dissection were done as previously described[58, 59]. In brief, horizontal slices (thickness = 300 μm) were cut with a vibratome (Leica VT S1000) in ice-cold cutting solution containing (in mM): 83 NaCl, 2.5 KCl, 0.5 $CaCl_2$, 3.3 $MgSO_4$, 26.2 $NaHCO_3$, 1 NaH_2PO_4, 22 D-glucose and 72 sucrose. Slices were transferred to normal ACSF at ~34°C for 30 min and then stored at room temperature before the experiment. The normal ACSF

used during recordings contained (in mM): 124 NaCl, 3 KCl, 2 $CaCl_2$, 1.3 $MgSO_4$, 26 $NaHCO_3$, 1.25 NaH_2PO_4, 10 D-glucose with osmolarity of 300 mOsm and pH = 7.4 when bubbled with 95% O_2-5% CO_2. Individual slices were transferred to the recording chamber and perfused with oxygenated ACSF. All recordings were performed at 37°C (± 0.5°C)

Whole cell and cell-attached recordings were performed using an IR-DIC microscope (Olympus BX51). Recordings were performed using borosilicate glass pipettes with resistance of 4-8 MΩ and filled with an intracellular solution (mM) containing: 110 K-gluconate, 10 KCl, 10 HEPES, 4 ATP, 0.3 GTP, 10 phosphocreatine and 0.4% biocytin and pH between 7.2 and 7.3. Recordings were amplified using Multiclamp 700A amplifiers (Molecular devices, USA), filtered at 4 KHz, digitized (5-20 KHz), and acquired using PulseQ electrophysiology package running on Igor Pro (Wavemetrics, USA).

ON stimulation was achieved using a bipolar electrode. The ON was identified under DIC and the electrode was placed on the nerve, in the vicinity of the glomerulus in which the VGLUT3 neuron projected its apical dendrite. The electrical stimuli (200 μs) were delivered at 0.33 Hz using an isolated Pulse stimulator (AM-systems).

For optogenetic experiments, we stimulated Vglut3-ChR2 neurons with a LED (Thorlabs, Germany, 2-10ms pulse) replacing the halogen light source transmission of the microscope. All recorded neurons kept for the connectivity analysis had intact dendritic arborizations (e.g. intact primary and secondary dendrites for M/T cells). The power after the objective was set to 0.6-0.8 mW × mm^2 and maintained constant during the experiments. The objective (Olympus, LUMPLFLN 40XW, Numerical aperture=0.8 and working distance = 3.33 mm) was positioned either on top of the glomerular layer, external plexiform layer or granule cell layer (different locations have been tested during the recordings of the same cell). During photobleaching experiments (light on for an hour), we estimated that the beached area had a diameter of ~300-400 μm. However, during short pulse of light illumination (2-10ms), the area efficiently recruiting ChR2-expressing cells may be smaller.

2,3-dioxo-6-nitro-1,2,3,4-tetrahydrobenzo[*f*]quinoxaline-7-sulfonamide disodium salt (NBQX), dl-2-amino-5-phosphonovaleric acid (APV), SR-95531 (gabazine), (3-Aminopropyl)(diethoxymethyl)phosphinic acid (CGP 35348), 5HT hydrochloride (5-HT), 4-(4-fluorobenzoyl)-1-(4-phenylbutyl) piperidine oxalate (4F 4PP), (4-Bromo-3,6-dimethoxybenzocyclobuten-1-yl) methylamine hydrobromide (TCB-2), (RS)-Baclofen and ZD7288 were purchased from Tocris (Bristol, UK). All salts and (R)-(-)-Apomorphine hydrochloride was purchased from Sigma Aldrich (Germany).

Data processing and analysis was done using Igor (Wavemetrics), Matlab (Mathworks) and Excel (Microsoft, Office). Data are reported as mean ± s.e.m.

To confirm the identity of recorded neurons, either 1 mM Alexa 488 hydrazide or 1 mM Alexa 568 hydrazide (Invitrogen) was included in the intracellular solution. Following recordings, slices were fixed in 4% PFA for 2 hours. Biocytin staining was used to analyze neurons morphology. Briefly, slices were fixed for 3 hours in phosphate buffer (pH 7.4) containing 4% PAF. Thereafter, slices were transferred into phosphate-buffered saline (PBS) containing 3% H_2O_2 to block endogenous peroxidases. After rinsing, slices were incubated

Europe PMC Funders Author Manuscripts

for 2 h with avidin-biotin complex. The samples were then rinsed again and developed with diaminobenzidine under bright-field microscope until the cells were visible. The reaction was stopped transferring the slices in PBS. Finally, slices were mounted on slides using 85% glycerol. Cells were reconstructed in bright field under a 100×/1.30 NA oil immersion objective using Neurolucida system (MicroBrightField).

Some slices containing juxtaglomerular neurons receiving direct inhibitory connection from Vglut3-ChR2 cells were fixed in 4% PAF as describe above and immunostaining for VGLUT2 (1:1000, Synaptic systems, cat. num. 135403) was performed in 300 μm the slices. Slices were incubated with TBSTT at least for 6 hours to maximize antibodies penetration.

Odorants and stimulation

The odorants used were methyl benzoate (MB, ≥98% purity), amyl acetate (AA, ≥99%), ethyl butyrate (EB, ≥99%), Carvone – (C–, >95%), 3-Hexanone (Hx, ≥98% purity). All chemicals were obtained from Sigma-Aldrich or Fluka Chemie (Steinheim, Germany). Odorants were delivered through a custom made olfactometer during an animal's expiration as described previously[34, 60]. The air flow passed through the vials containing the odorants. The total flow was constant (0.4 l/min). To maintain a stable odor concentration during the entire stimulus application, we ensured that flows were stationary with a 5 s preloading before the odorant was delivered.

2-photon calcium imaging

Three to four month–old Vglut3-GCaMP3 mice were anesthetized with an intraperitoneal injection of a mixture of midazolam (0.4 mg/kg), medetomidine (2 mg/kg) and fentanyl (100 μg/kg). By placing the mouse on a custom made heating pad we monitored body temperature. Animals were implanted with a stainless steel head-post that was firmly attached to the skull with dental cement (Syntac Assortment, Ivoclar Vivadent Clinical, Liechtenstien). A cranial window of 2.5 mm diameter was then drilled on the central part of the olfactory bulb in order to avoid damages to the blood vessels located under caudal part of the bone that overly the structure. A 3 mm coverglass was then sealed on top of the craniotomy with dental cement. To reverse the anesthesia, animals were injected subcutaneously with a mixture of flumazenil (4 mg/kg), naloxone (0.8 mg/kg) and atipamezole (20 mg/kg). All mice were allowed to recover for 7 days after surgery and then trained for 7 days to be head-restrained.

To perform calcium imaging in awake mice, we used a 20× Olympus objective (0.95 NA) mounted on a custom made microscope controlled with *ScanImage*[61] (http://www.scanimage.org). GCaMP3 was excited using a Ti-Sapphire laser (Chameleon ultra II, Coherent) tuned to λ = 910 nm. The field of view was 200 × 200 μm and images were acquired at a resolution of 512 × 128 and a frequency of 7.81 Hz. The imaging protocol consisted of a series of 20 trials corresponding to 20 successive odor applications. The breathing cycle was monitored during imaging sessions and used to synchronize odor application onset to the end of animals' inspiration via a slope/height window discriminator (FHC, Bowdoinham, USA). Each trial lasted approximately 17 seconds with 5 s odor

preloading (odorant stream bypassing the animal), a 200ms delay period during which the breathing cycle could trigger odor delivery, a 2s odor application and a 10s post odor period.

Images were analyzed offline using Image J and custom analysis routine written in Matlab. Briefly, circular regions of interest (ROIs) were placed on GCaMP3 expressing cells to extract their changes in fluorescence intensity over time. For each ROI, the change in fluorescence relative to baseline (ΔF/F) was calculated and filtered with a 3 point moving average filter. A cell was considered responsive when a Ca^{2+} change was detected in more than 10 trials out of 20 and within a time window 0-2 s after odor onset. We set a threshold for detecting evoked Ca^{2+} responses as 2σ where σ is the standard deviation calculated over 5s baseline activity before odor onset.

Statistical analysis

In this study, we used ANOVA and post-hoc test, two tailed paired and unpaired t-test, χ^2 test and different non-parametric tests (see text and legends). Shapiro-Wilk test was used to assess normality of the data. For all parametric ANOVA, homogeneity of variance was tested using Levene's test or a test of sphericity (for one-way repeated measures ANOVA).

No animal, cell or outlier has been excluded from the dataset.

In vivo electrophysiology

The initial animal preparation, recording procedure and spike sorting analysis have been extensively presented elsewhere[33, 34, 62]. For all experiments, respiration was monitored using a directional air flow sensor (AWM2100V, Honeywell, MN) placed in front of the mouse snout. This sensor did not occlude the mouse nose and indeed did not stop the odor from reaching the nostrils. Three month-old Vglut3-ChR2 and C57Bl6J mice were anesthetized with an intraperitoneal injection of a mixture of midazolam (0.4 mg/kg), medetomidine (2 mg/kg) and fentanyl (100 μg/kg). A 1-2 mm window was drilled above the OB and the dura mater was opened. One silicon-based recording optrode (A1x32-Poly3-5mm-50s-177-OA32, NeuroNexus Technologies, Ann Arbor, MI, USA) was inserted. Photostimulation was done by connecting the optrode to a fiber coupled blue laser (SDL-473-050MFL, Shangai dreamlasers, Shangai, China). For all recordings, the laser power was set such that the power at the end of the fiber connected to the laser head was 20mW. Photostimulation consisted of a train of 60 light pulses (10 ms pulse, 50Hz) synchronized to odor onset. The skull cavity was filled with an ophthalmic gel (Lacryvisc, Alcon) to protect the brain from drying. A silver wire contacting the gel was connected to the air table to ground the preparation.

Electrodes were lowered vertically in the target zone until the mitral/tufted cell layer was reached. It must be noted that our recording electrodes had low impedances (1–4 MΩ at 1 kHz). Stability and reasonable size of the extracellular spike with respect to background noise are two necessary conditions for single-cell identification (clustering, see below), which in the case of low impedance electrodes could only be fulfilled by mitral and tufted cells (the larger cells in the OB), as observed by others[33, 35, 63-66]. Further details about recording and spike sorting have been described extensively elsewhere[33, 34]. In brief, wide-band field potentials were amplified (100×) and band-pass filtered (0.1 Hz to 9 kHz). All

data was digitized at 32556 Hz with the Cheetah Digital Lynx system (Neuralynx, Tucson, AZ). Spikes were detected by a threshold on the high-pass filtered signal, decomposed in 16 features, and automatically clustered by the KlustaKwick software[67]. Obtained clusters were manually merged in Klusters software[68] when they showed a clear refractory period in the cross-correlation of their spike trains. Individual neurons were finally identified as the clusters showing a clean refractory period in their autocorrelation. All subsequent analyses and statistics were calculated using custom scripts written for Matlab (MathWorks, Inc., Natick, MA).

Fifteen trials for each condition (8 conditions: spontaneous and 3 odorants tested with and without photostimulation) have been used. All trials for different conditions have been presented randomly. To characterize the effect of photostimulation, we calculated each cell's firing during spontaneous and odor application by computing the average firing rate on the first two breathing cycles following stimulus onset (for spontaneous firing, no odor was applied). We compared the firing rate with and without photostimulation using the sign test.

Supplementary Material

Refer to Web version on PubMed Central for supplementary material.

ACKNOWLEDGEMENTS

We thank Anthony Holtmaat for helping setting up the 2-photon microscope and for helpful discussions. We thank Sidney Simon, Michael Patterson and members of the Carleton laboratory for helpful discussions and comments on the manuscript. This research was supported by the University of Geneva, the European Research Council (contract number ERC-2009-StG-243344-NEUROCHEMS, A.C:), the Swiss National Science Foundation (SNF professor grant numbers: PP0033_119169 and PP00P3_139189 to A.C., grants CR33I13_143723 to A.C. and I.R. and 31003A_149753 to I.R.), the National Center of Competence in Research (NCCR) "SYNAPSY - The Synaptic Bases of Mental Diseases" financed by the Swiss National Science Foundation (n° 51AU40_125759, A.C.), the Novartis foundation for medical research (A.C.), the Carlos & Elsie de Reuter foundation (A.C.), the Ernst & Lucie Schmidheiny foundation (A.C.) and the European Molecular Biology Organization (young investigator program, A.C.).

REFERENCES

1. Ressler KJ, Sullivan SL, Buck LB. Information coding in the olfactory system: evidence for a stereotyped and highly organized epitope map in the olfactory bulb. Cell. 1994; 79:1245–1255. [PubMed: 7528109]
2. Vassar R, et al. Topographic organization of sensory projections to the olfactory bulb. Cell. 1994; 79:981–991. [PubMed: 8001145]
3. De Saint Jan D, Hirnet D, Westbrook GL, Charpak S. External tufted cells drive the output of olfactory bulb glomeruli. J Neurosci. 2009; 29:2043–2052. [PubMed: 19228958]
4. Gire DH, Schoppa NE. Control of on/off glomerular signaling by a local GABAergic microcircuit in the olfactory bulb. J Neurosci. 2009; 29:13454–13464. [PubMed: 19864558]
5. Najac M, De Saint Jan D, Reguero L, Grandes P, Charpak S. Monosynaptic and polysynaptic feed-forward inputs to mitral cells from olfactory sensory neurons. J Neurosci. 2011; 31:8722–8729. [PubMed: 21677156]
6. Gire DH, et al. Mitral cells in the olfactory bulb are mainly excited through a multistep signaling path. J Neurosci. 2012; 32:2964–2975. [PubMed: 22378870]
7. Bellocchio EE, Reimer RJ, Fremeau RT Jr. Edwards RH. Uptake of glutamate into synaptic vesicles by an inorganic phosphate transporter. Science. 2000; 289:957–960. [PubMed: 10938000]

8. Takamori S, Rhee JS, Rosenmund C, Jahn R. Identification of a vesicular glutamate transporter that defines a glutamatergic phenotype in neurons. Nature. 2000; 407:189–194. [PubMed: 11001057]
9. Aihara Y, et al. Molecular cloning of a novel brain-type Na(+)-dependent inorganic phosphate cotransporter. Journal of neurochemistry. 2000; 74:2622–2625. [PubMed: 10820226]
10. Bai L, Xu H, Collins JF, Ghishan FK. Molecular and functional analysis of a novel neuronal vesicular glutamate transporter. J Biol Chem. 2001; 276:36764–36769. [PubMed: 11432869]
11. Fremeau RT Jr. et al. The expression of vesicular glutamate transporters defines two classes of excitatory synapse. Neuron. 2001; 31:247–260. [PubMed: 11502256]
12. Herzog E, et al. The existence of a second vesicular glutamate transporter specifies subpopulations of glutamatergic neurons. J Neurosci. 2001; 21:RC181. [PubMed: 11698619]
13. Fremeau RT Jr. et al. The identification of vesicular glutamate transporter 3 suggests novel modes of signaling by glutamate. Proceedings of the National Academy of Sciences of the United States of America. 2002; 99:14488–14493. [PubMed: 12388773]
14. Gras C, et al. A third vesicular glutamate transporter expressed by cholinergic and serotoninergic neurons. J Neurosci. 2002; 22:5442–5451. [PubMed: 12097496]
15. Schafer MK, Varoqui H, Defamie N, Weihe E, Erickson JD. Molecular cloning and functional identification of mouse vesicular glutamate transporter 3 and its expression in subsets of novel excitatory neurons. J Biol Chem. 2002; 277:50734–50748. [PubMed: 12384506]
16. Takamori S, Malherbe P, Broger C, Jahn R. Molecular cloning and functional characterization of human vesicular glutamate transporter 3. EMBO reports. 2002; 3:798–803. [PubMed: 12151341]
17. Nakamura K, Hioki H, Fujiyama F, Kaneko T. Postnatal changes of vesicular glutamate transporter (VGluT)1 and VGluT2 immunoreactivities and their colocalization in the mouse forebrain. J Comp Neurol. 2005; 492:263–288. [PubMed: 16217795]
18. Ohmomo H, et al. Postnatal changes in expression of vesicular glutamate transporters in the main olfactory bulb of the rat. Neuroscience. 2009; 160:419–426. [PubMed: 19264112]
19. Gabellec MM, Panzanelli P, Sassoe-Pognetto M, Lledo PM. Synapse-specific localization of vesicular glutamate transporters in the rat olfactory bulb. The European journal of neuroscience. 2007; 25:1373–1383. [PubMed: 17425564]
20. Kosaka T, Kosaka K. Heterogeneity of calbindin-containing neurons in the mouse main olfactory bulb: I. General description. Neurosci Res. 2010; 67:275–292. [PubMed: 20406658]
21. Kosaka K, Kosaka T. Chemical properties of type 1 and type 2 periglomerular cells in the mouse olfactory bulb are different from those in the rat olfactory bulb. Brain Res. 2007; 1167:42–55. [PubMed: 17662264]
22. Hayar A, Karnup S, Shipley MT, Ennis M. Olfactory bulb glomeruli: external tufted cells intrinsically burst at theta frequency and are entrained by patterned olfactory input. J Neurosci. 2004; 24:1190–1199. [PubMed: 14762137]
23. Liu S, Shipley MT. Multiple conductances cooperatively regulate spontaneous bursting in mouse olfactory bulb external tufted cells. J Neurosci. 2008; 28:1625–1639. [PubMed: 18272683]
24. Hayar A, Karnup S, Ennis M, Shipley MT. External tufted cells: a major excitatory element that coordinates glomerular activity. J Neurosci. 2004; 24:6676–6685. [PubMed: 15282270]
25. Hayar A, Shipley MT, Ennis M. Olfactory bulb external tufted cells are synchronized by multiple intraglomerular mechanisms. J Neurosci. 2005; 25:8197–8208. [PubMed: 16148227]
26. McQuiston AR, Katz LC. Electrophysiology of interneurons in the glomerular layer of the rat olfactory bulb. Journal of neurophysiology. 2001; 86:1899–1907. [PubMed: 11600649]
27. Antal M, Eyre M, Finklea B, Nusser Z. External tufted cells in the main olfactory bulb form two distinct subpopulations. The European journal of neuroscience. 2006; 24:1124–1136. [PubMed: 16930438]
28. Macrides F, Schneider SP. Laminar organization of mitral and tufted cells in the main olfactory bulb of the adult hamster. J Comp Neurol. 1982; 208:419–430. [PubMed: 7119169]
29. Liu S, Aungst JL, Puche AC, Shipley MT. Serotonin modulates the population activity profile of olfactory bulb external tufted cells. Journal of neurophysiology. 2012; 107:473–483. [PubMed: 22013233]

30. Hsia AY, Vincent JD, Lledo PM. Dopamine depresses synaptic inputs into the olfactory bulb. Journal of neurophysiology. 1999; 82:1082–1085. [PubMed: 10444702]
31. Wachowiak M, et al. Inhibition [corrected] of olfactory receptor neuron input to olfactory bulb glomeruli mediated by suppression of presynaptic calcium influx. Journal of neurophysiology. 2005; 94:2700–2712. [PubMed: 15917320]
32. Nickell WT, Behbehani MM, Shipley MT. Evidence for GABAB-mediated inhibition of transmission from the olfactory nerve to mitral cells in the rat olfactory bulb. Brain research bulletin. 1994; 35:119–123. [PubMed: 7953767]
33. Bathellier B, Buhl DL, Accolla R, Carleton A. Dynamic ensemble odor coding in the mammalian olfactory bulb: sensory information at different timescales. Neuron. 2008; 57:586–598. [PubMed: 18304487]
34. Gschwend O, Beroud J, Carleton A. Encoding odorant identity by spiking packets of rate-invariant neurons in awake mice. PLoS ONE. 2012; 7:e30155. [PubMed: 22272291]
35. Patterson MA, Lagier S, Carleton A. Odor representations in the olfactory bulb evolve after the first breath and persist as an odor afterimage. Proceedings of the National Academy of Sciences of the United States of America. 2013; 110:E3340–3349. [PubMed: 23918364]
36. Fremeau RT Jr. et al. Vesicular glutamate transporters 1 and 2 target to functionally distinct synaptic release sites. Science. 2004; 304:1815–1819. [PubMed: 15118123]
37. Mendez JA, et al. Developmental and target-dependent regulation of vesicular glutamate transporter expression by dopamine neurons. J Neurosci. 2008; 28:6309–6318. [PubMed: 18562601]
38. Noh J, Seal RP, Garver JA, Edwards RH, Kandler K. Glutamate co-release at GABA/glycinergic synapses is crucial for the refinement of an inhibitory map. Nature neuroscience. 2010; 13:232–238. [PubMed: 20081852]
39. Brill MS, et al. Adult generation of glutamatergic olfactory bulb interneurons. Nature neuroscience. 2009; 12:1524–1533. [PubMed: 19881504]
40. Carleton A, Petreanu LT, Lansford R, Alvarez-Buylla A, Lledo PM. Becoming a new neuron in the adult olfactory bulb. Nature neuroscience. 2003; 6:507–518. [PubMed: 12704391]
41. Carleton A, et al. Making scents of olfactory neurogenesis. J Physiol Paris. 2002; 96:115–122. [PubMed: 11755790]
42. Winpenny E, et al. Sequential generation of olfactory bulb glutamatergic neurons by Neurog2-expressing precursor cells. Neural development. 2011; 6:12. [PubMed: 21466690]
43. El Mestikawy S, Wallen-Mackenzie A, Fortin GM, Descarries L, Trudeau LE. From glutamate co-release to vesicular synergy: vesicular glutamate transporters. Nat Rev Neurosci. 2011; 12:204–216. [PubMed: 21415847]
44. Boulland JL, et al. Expression of the vesicular glutamate transporters during development indicates the widespread corelease of multiple neurotransmitters. J Comp Neurol. 2004; 480:264–280. [PubMed: 15515175]
45. Somogyi J, et al. GABAergic basket cells expressing cholecystokinin contain vesicular glutamate transporter type 3 (VGLUT3) in their synaptic terminals in hippocampus and isocortex of the rat. The European journal of neuroscience. 2004; 19:552–569. [PubMed: 14984406]
46. Shutoh F, Ina A, Yoshida S, Konno J, Hisano S. Two distinct subtypes of serotonergic fibers classified by co-expression with vesicular glutamate transporter 3 in rat forebrain. Neurosci Lett. 2008; 432:132–136. [PubMed: 18222609]
47. Kao YH, et al. Evidence that certain retinal bipolar cells use both glutamate and GABA. J Comp Neurol. 2004; 478:207–218. [PubMed: 15368537]
48. Kato HK, Gillet SN, Peters AJ, Isaacson JS, Komiyama T. Parvalbumin-expressing interneurons linearly control olfactory bulb output. Neuron. 2013; 80:1218–1231. [PubMed: 24239124]
49. Miyamichi K, et al. Dissecting local circuits: parvalbumin interneurons underlie broad feedback control of olfactory bulb output. Neuron. 2013; 80:1232–1245. [PubMed: 24239125]
50. Fukunaga I, Berning M, Kollo M, Schmaltz A, Schaefer AT. Two distinct channels of olfactory bulb output. Neuron. 2012; 75:320–329. [PubMed: 22841316]
51. Igarashi KM, et al. Parallel mitral and tufted cell pathways route distinct odor information to different targets in the olfactory cortex. J Neurosci. 2012; 32:7970–7985. [PubMed: 22674272]

52. Petzold GC, Hagiwara A, Murthy VN. Serotonergic modulation of odor input to the mammalian olfactory bulb. Nature neuroscience. 2009; 12:784–791. [PubMed: 19430472]
53. Grimes WN, Seal RP, Oesch N, Edwards RH, Diamond JS. Genetic targeting and physiological features of VGLUT3+ amacrine cells. Visual neuroscience. 2011; 28:381–392. [PubMed: 21864449]
54. Madisen L, et al. A robust and high-throughput Cre reporting and characterization system for the whole mouse brain. Nature neuroscience. 2010; 13:133–140. [PubMed: 20023653]
55. Madisen L, et al. A toolbox of Cre-dependent optogenetic transgenic mice for light-induced activation and silencing. Nature neuroscience. 2012; 15:793–802. [PubMed: 22446880]
56. Zariwala HA, et al. A Cre-dependent GCaMP3 reporter mouse for neuronal imaging in vivo. J Neurosci. 2012; 32:3131–3141. [PubMed: 22378886]
57. Tamamaki N, et al. Green fluorescent protein expression and colocalization with calretinin, parvalbumin, and somatostatin in the GAD67-GFP knock-in mouse. J Comp Neurol. 2003; 467:60–79. [PubMed: 14574680]
58. Castillo PE, Carleton A, Vincent JD, Lledo PM. Multiple and opposing roles of cholinergic transmission in the main olfactory bulb. J Neurosci. 1999; 19:9180–9191. [PubMed: 10531421]
59. Didier A, et al. A dendrodendritic reciprocal synapse provides a recurrent excitatory connection in the olfactory bulb. Proceedings of the National Academy of Sciences of the United States of America. 2001; 98:6441–6446. [PubMed: 11353824]
60. Bathellier B, Van De Ville D, Blu T, Unser M, Carleton A. Wavelet-based multi-resolution statistics for optical imaging signals: Application to automated detection of odour activated glomeruli in the mouse olfactory bulb. Neuroimage. 2007; 34:1020–1035. [PubMed: 17185002]
61. Pologruto TA, Sabatini BL, Svoboda K. ScanImage: flexible software for operating laser scanning microscopes. Biomedical engineering online. 2003; 2:13. [PubMed: 12801419]
62. Vincis R, Gschwend O, Bhaukaurally K, Beroud J, Carleton A. Dense representation of natural odorants in the mouse olfactory bulb. Nature neuroscience. 2012; 15:537–539. [PubMed: 22406552]
63. Rinberg D, Koulakov A, Gelperin A. Sparse odor coding in awake behaving mice. J Neurosci. 2006; 26:8857–8865. [PubMed: 16928875]
64. Fantana AL, Soucy ER, Meister M. Rat olfactory bulb mitral cells receive sparse glomerular inputs. Neuron. 2008; 59:802–814. [PubMed: 18786363]
65. Cury KM, Uchida N. Robust odor coding via inhalation-coupled transient activity in the mammalian olfactory bulb. Neuron. 2010; 68:570–585. [PubMed: 21040855]
66. Shusterman R, Smear MC, Koulakov AA, Rinberg D. Precise olfactory responses tile the sniff cycle. Nature neuroscience. 2011; 14:1039–1044. [PubMed: 21765422]
67. Harris KD, Henze DA, Csicsvari J, Hirase H, Buzsaki G. Accuracy of tetrode spike separation as determined by simultaneous intracellular and extracellular measurements. Journal of neurophysiology. 2000; 84:401–414. [PubMed: 10899214]
68. Hazan L, Zugaro M, Buzsaki G. Klusters, NeuroScope, NDManager: a free software suite for neurophysiological data processing and visualization. Journal of neuroscience methods. 2006; 155:207–216. [PubMed: 16580733]

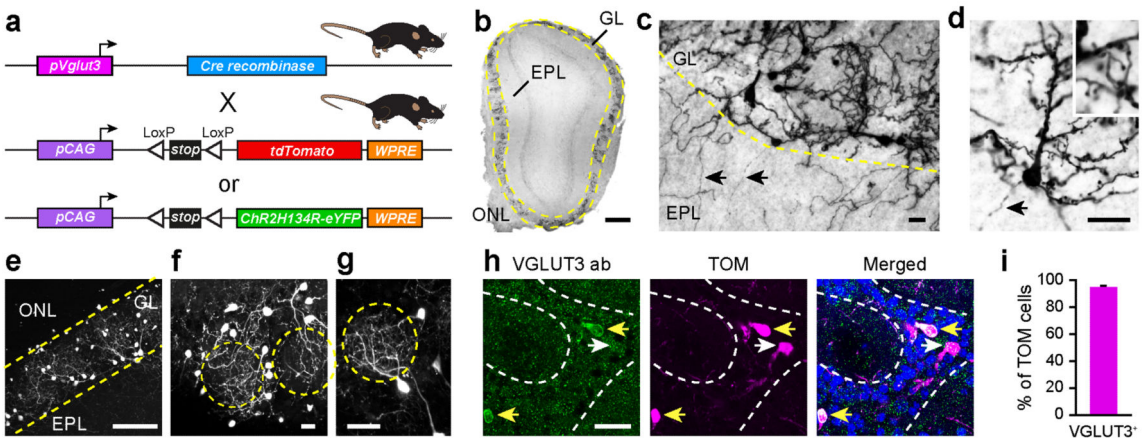

Figure 1. VGLUT3 expression defines a neuronal population located in the glomerular layer of the mouse olfactory bulb

(**a**) Schema of the breeding strategy. A transgenic mouse expressing Cre recombinase under the *Vglut3* promoter (*pVglut3*) was crossed with two reporter lines conditionally expressing either tdTomato or Channelrhodopsin2-YFP. pCAG: *CAG* promoter, *WPRE*: Woodchuck hepatitis Post-transcriptional Regulatory Element, *LoxP*: sequence recognized by the Cre recombinase for recombination. (**b-d**) Coronal sections of the adult OB immunostained for YFP in Vglut3-ChR2 mice. Positive cell bodies were found exclusively in the glomerular layer (**b**, GL, *left image*). Stained cells often exhibited axons (*black arrows*, **c,d**) and spiny dendrites (**d**). (**e-g**) Z-stack projections of TOM^+ neurons imaged in the GL using 2-photon microscopy in 300 μm thick slices of a Vglut3-TOM mouse. The dendritic tuft of TOM^+ cells extensively arborized individual glomeruli (circular dotted lines in **f,g**). Some cells had longer dendrites than others (**g**). ONL: olfactory nerve layer, EPL: external plexiform layer. (**h**) Antibody staining for VGLUT3 on Vglut3-TOM slices. Arrows highlight TOM^+ neurons expressing VGLUT3 (*yellow*) or not (*white*). (**i**) Percentage of TOM^+ cells stained by the VGLUT3 antibody in two month old animals (n = 4 mice, data are shown as mean ± s.e.m). Scale bars: 0.3 mm (**b**), 0.1 mm (**e**) and 20 μm (**c,d,f-h**).

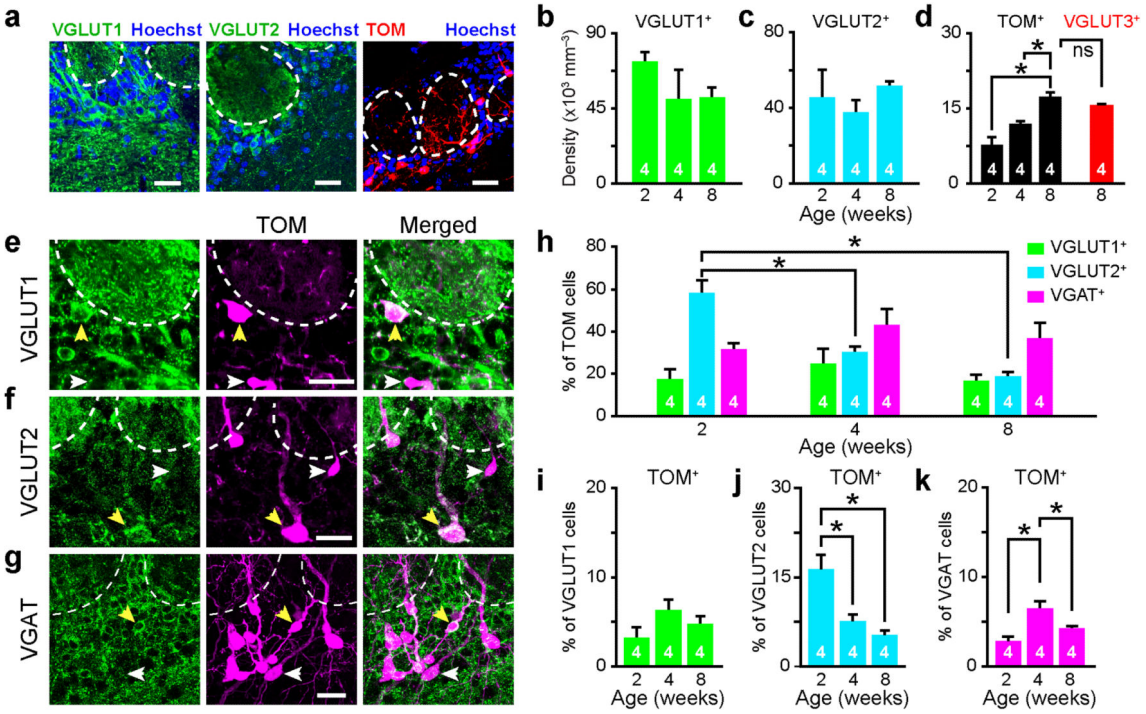

Figure 2. Vesicular glutamate and GABA transporters define different subpopulations of VGLUT3 neurons

(**a**) Confocal images of the glomerular layer in OB slices taken from Vglut3-TOM mice and immunostained for VGLUT1 or VGLUT2. Glomeruli boundaries (*dotted lines*) were visualized by Hoechst staining. (**b-d**) Age-dependent variation in density of neurons expressing different vesicular transporters in the glomerular layer (Kruskal-Wallis ANOVA $H(2,12) = 3.5$, $P = 0.17$ for VGLUT1$^+$ and one way ANOVA $F(2,9) = 1.35$, $P = 0.3$; $F(2,9) = 0.55$, $P = 0.59$; $F(2,9) = 10.74$, $P = 0.004$ for, VGLUT2$^+$ and TOM$^+$, respectively). Post-hoc Fischer least significant difference (LSD) test in **d**: 2 *vs.* 4 weeks $P = 0.06$, 2 *vs.* 8 weeks $^*P = 0.002$, 4 *vs.* 8 weeks $^*P = 0.04$. TOM$^+$ and VGLUT3$^+$ density was not statistically different (Unpaired t-test $t(1.9)$, P=0.13). (**e-g**) Confocal images showing co-localization (*yellow arrows*) and no co-localization (*white arrows*) of TOM with VGLUT1 (**e**), VGLUT2 (**f**) or VGAT (**g**). (**h**) Percentage of TOM$^+$ cells expressing VGLUT1, VGLUT2 or VGAT (one way ANOVA $F(2,9) = 0.67$, $P = 0.53$; $F(2,9) = 26.3$, $P = 2.10^{-4}$; $F(2,9) = 0.91$, $P = 0.44$ for VGLUT1$^+$, VGLUT2$^+$ and VGAT$^+$, respectively). LSD test for VGLUT2$^+$: 2 *vs.* 4 weeks $^*P = 7.10^{-4}$, 2 *vs.* 8 weeks $^*P = 6.10^{-5}$, 4 *vs.* 8 weeks $P = 0.07$. (**i-k**) Percentage of VGLUT1$^+$ (**i**), VGLUT2$^+$ (**j**) or VGAT$^+$ (**k**) cells co-localized with TOM (one way ANOVA $F(2,9) = 2.1$, $P = 0.18$; $F(2,9) = 12.5$, $^*P = 0.003$; $F(2,9) = 14.4$, $^*P = 0.005$ for VGLUT1/TOM, VGLUT2/TOM, respectively and Kruskal-Wallis ANOVA $H(2,12) = 8.8$, $P = 0.013$ for VGAT/TOM). LSD test in **j:** 2 vs. 4 weeks $^*P = 0.005$, 2 vs. 8 weeks $^*P = 0.001$, 4 vs. 8 weeks $P = 0.35$; Kruskal-Wallis test in **k**: 2 vs. 4 weeks $^*P = 0.01$, 2 vs. 8 weeks $P = 0.71$, 4 vs. 8 weeks $P = 0.23$. Data are presented as mean ± s.e.m. (white numbers on histograms indicate number of mice). Scale bars: 20 μm.

Europe PMC Funders Author Manuscripts

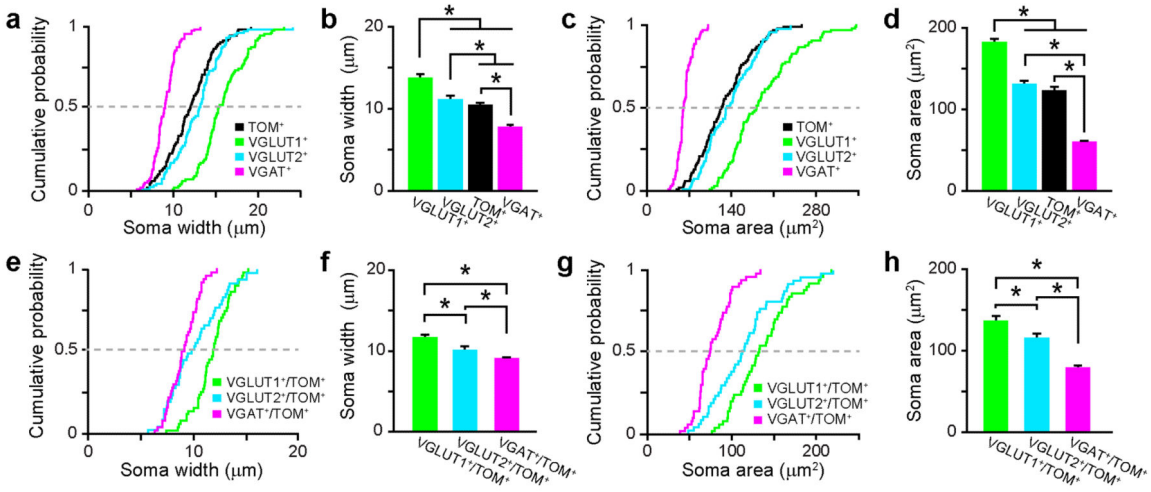

Figure 3. Different populations of glutamatergic neurons in the glomerular area differ in soma size

(**a**) Cumulative distribution ($\tilde{n}$ = 100 cells taken from 5-6 slices from 4 animals) of soma width measured in different cell populations. All distributions except TOM^+ *vs.* $VGLUT2^+$ are significantly different (Kolmogorov-Smirnov KS test $P < 0.001$). (**b**) Average soma size measured in different populations of neurons. One way ANOVA $F(3,387) = 120.6$, $P < 10^{-8}$,: post hoc LSD test: VGLUT1 *vs.* VGLUT2 $*P = 8.1\times10^{-15}$, VGLUT3 *vs.* VGLUT1 $*P = 2.8\times10^{-23}$, VGLUT3 *vs.* VGLUT2 $*P = 0.01$, VGAT *vs.* VGLUT1 $*P = 9.5\times10^{-57}$, VGAT *vs.* VGLUT2 $*P = 8.2\times10^{-23}$, VGAT *vs.* VGLUT3 $*P = 2.5\times10^{-15}$. (**c**) Cumulative distribution of soma area in the same populations of neurons. All distributions except TOM^+ *vs.* $VGLUT2^+$ are significantly different (KS test $P < 0.001$). (**d**) Average soma area measured in different population of neurons. One way ANOVA $F(3,387) = 15$, $P < 10^{-8}$, post hoc LSD test: VGLUT2 *vs.* VGLUT1 $*P = 3.4\times10^{-17}$, VGLUT3 *vs.* VGLUT1 $*P = 6.1\times10^{-22}$, VGLUT3 *vs.* VGLUT2 $P = 0.2$, VGAT *vs.* VGLUT1 $*P = 1.10^{-57}$, VGAT *vs.* VGLUT2 $*P = 2.4\times10^{-29}$, VGAT *vs.* VGLUT3 $*P = 4.2\times10^{-25}$. (**e**) Cumulative distribution of soma width measured in different subpopulations of TOM^+ neurons co-expressing different vesicular transporters (n = 50 cells taken from 5-6 slices from 4 animals). All distributions are significantly different (KS test at least $P < 0.001$). (**f**) Average soma width measured in different populations of neurons. One way ANOVA $F(2,138) = 21.4$, $*P = 7.8\times10^{-9}$. Post hoc Fischer LSD test: VGLUT2/TOM *vs.* VGLUT1/TOM $*P = 1.1\times10^{-4}$, VGAT/TOM *vs.* VGLUT1/TOM $*P = 1.4\times10^{-9}$, VGAT/TOM *vs.* VGLUT2/TOM $*P = 0.01$. (**g**) Cumulative distribution of soma area in the same populations of neurons. All distributions are significantly different (KS test $P < 0.001$). (**h**) Average soma area measured in different populations of neurons. One way ANOVA $F(2,138) = 35.3$, $P = 4.10^{-13}$. LSD test at least $*P = 0.002$. VGLUT2/TOM *vs.* VGLUT1/TOM $*P = 0.002$, VGAT/TOM *vs.* VGLUT1/TOM $*P = 7.3\times10^{-14}$, VGAT/TOM *vs.* VGLUT2/TOM $*P = 7.1\times10^{-7}$.

Europe PMC Funders Author Manuscripts

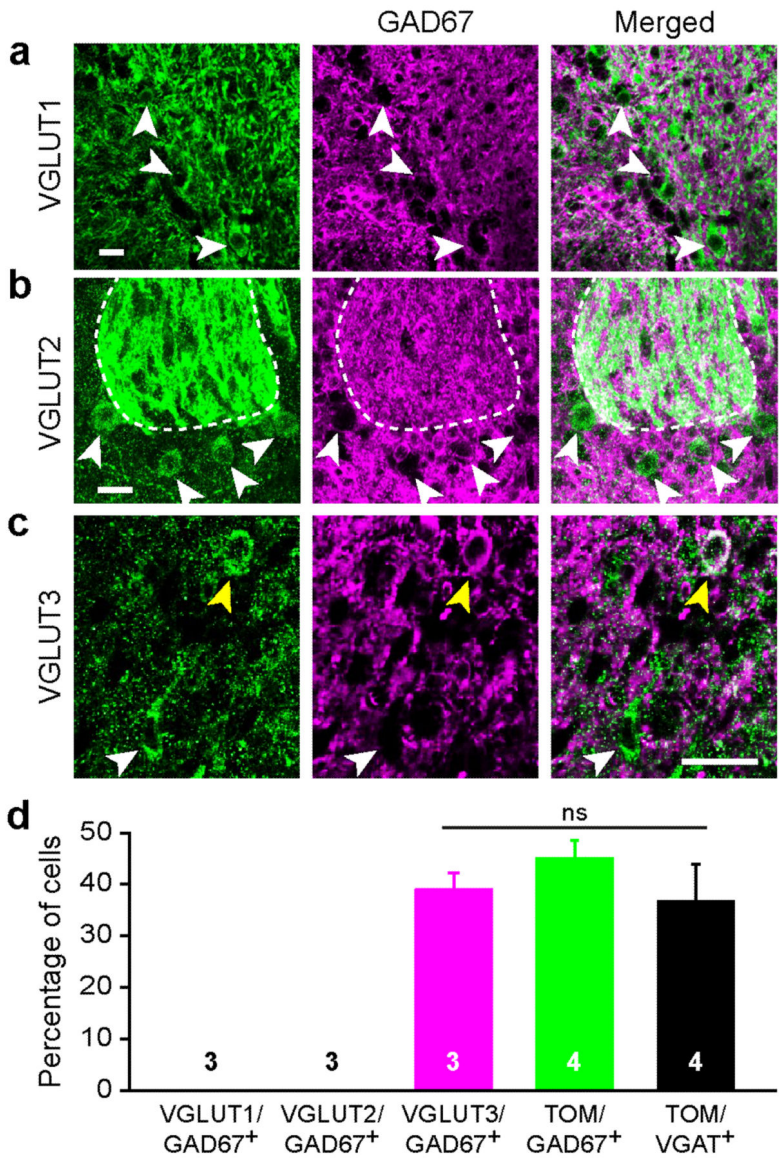

Figure 4. Neurons expressing VGLUT3 are the only glutamatergic neurons of the glomerular layer exhibiting a GABAergic phenotype

(**a-c**) Confocal images acquired from the glomerular layer of 2 month-old C57BL/6J mice double stained for VGLUT1 and GAD67 (**a**), VGLUT2 and GAD67 (**b**), VGLUT3 and GAD67 (**c**). Yellow and white arrows indicate co-stained and not co-stained cells, respectively. Scale bars: 20 μm. (**d**) Percentage of VGLUT1$^+$, VGLUT2$^+$ and VGLUT3$^+$ cells expressing GAD67. Note that the percentage of TOM$^+$/GAD67$^+$ and TOM$^+$/VGAT$^+$ neurons was not statistically different from VGLUT3$^+$/GAD67$^+$ expressing cells. One way ANOVA $F(3,11)= 0.6$, $P = 0.5$. Data are presented as mean ± s.e.m. Numbers on histograms indicate number of mice.

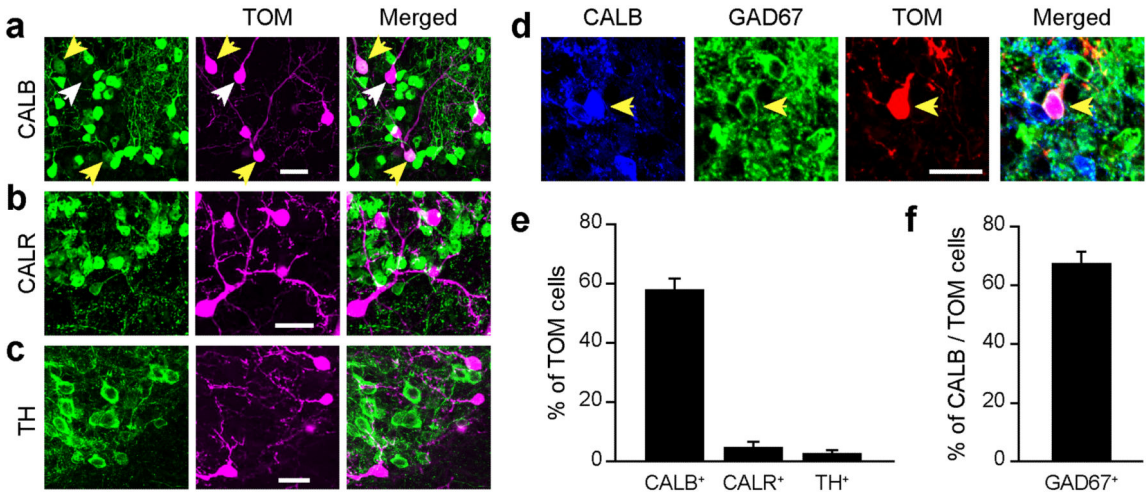

Figure 5. Immunohistochemical characterization of GABAergic VGLUT3 neurons

(**a-c**) Confocal images acquired from the glomerular layer of OB slices taken from Vglut3-TOM mice and immunostained for calbindin (CALB, **a**), calretinin (CALR, **b**) or tyrosine hydroxylase (TH, **c**). Arrows point to TOM^+ cells co-expressing (*yellow*) or not co-expressing (*white*) the tested marker. (**d**) Confocal images showing a TOM^+ cell co-expressing CALB and GAD67 (*yellow arrow*). (**e**) Percentage of TOM^+ cells expressing CALB, CALR or TH (n = 4 eight week old mice in each group; quantifications were done for each animal on ~100 cells imaged from ~6 slices). (**f**) Percentage of CALB/TOM cells expressing GAD67. Data are presented as mean ± s.e.m. Scale bars: 20 μm.

Europe PMC Funders Author Manuscripts

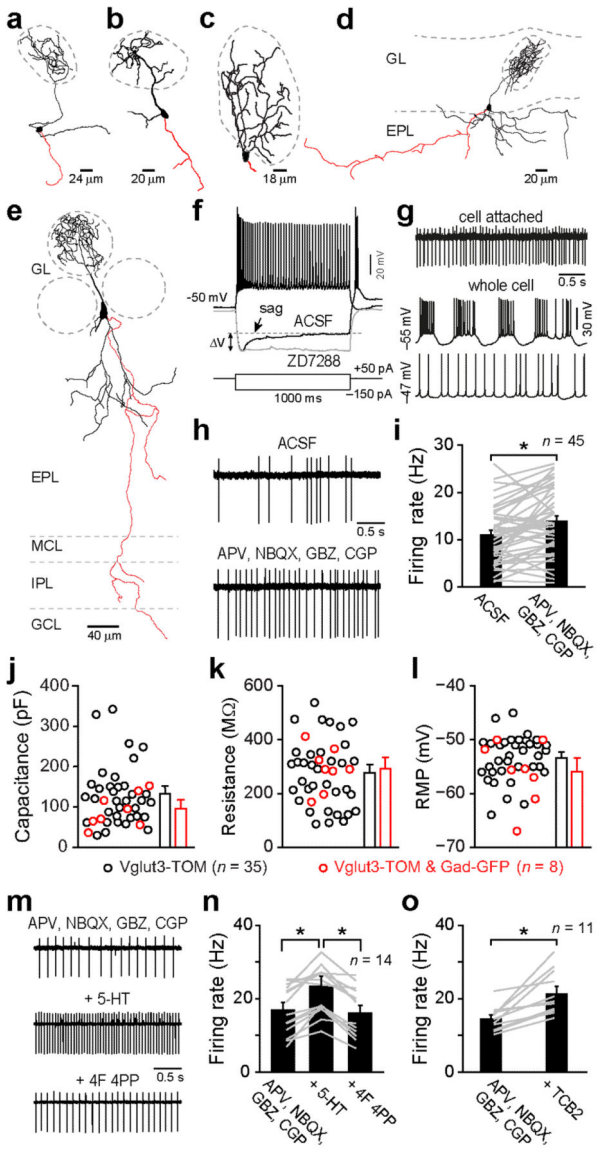

Figure 6. Vglut3 neurons exhibit electrophysiological properties of external tufted cells

(**a-e**) Morphology of Vglut3-TOM neurons patched and filled with biocytin (axons in red). IPL: internal plexiform layer. (**f**) Typical response of a TOM$^+$ neuron to injection of current pulses. Note the presence of sag (blocked by the specific I*h* current antagonist ZD7288 10 µM) and rebound spiking following hyperpolarization. ΔV: voltage difference between beginning and end of sag. (**g**) Spontaneous firing activity recorded from a TOM$^+$ neuron. Note the firing behavior depended on the resting membrane potential. (**h**) Vglut3-TOM neurons spontaneously fire in presence of 100 dl-APV, 10 NBQX, 10 SR-95531 (GBZ), 10 CGP 35348 (in µM, antagonists mix). (**i**) Summary graph showing the average firing frequency computed for different cells (from 45 slices from 25 animals) before and during drug application (*gray lines*: individual cell; $n = 45$, Wilcoxon matched pairs test $^*P = 0.0003$, $Z(44) = 3.65$). (**j-l**) Summary graphs showing single cells values and average for Vglut3-TOM (cells recorded in 9 mice) and Vglut3-TOM/Gad67-GFP neurons (cells

recorded in 2 mice) for capacitance (**j**, Mann-Whitney U test $P = 0.77$, $Z(41) = -0.3$), membrane resistance (**k**, Mann-Whitney U test $P = 0.22$, $Z(41) = 1.23$), resting membrane potential (**l**; RMP, Mann-Whitney U test $P = 0.35$, $Z(41) = 0.94$). (**m**) Spontaneous firing activity recorded from a TOM^+ neuron before and after sequential application of 40 μM 5-HT and the 5-HT2A receptor antagonist 4F-4PP (5 μM). (**n-o**) Summary graphs showing the average firing frequency computed for each cell (*grey lines*) or the population (*black bars*) during different drug conditions (**n**, one way repeated measures ANOVA $F(2,26) = 24.1$, $P = 1.3 \times 10^{-6}$; Post-hoc Fischer LSD test: drugs *vs.* 5HT $^*P = 10^{-7}$, $t(26) = 5.5$; 5HT *vs.* 4F4PP $^*P = 8.3 \times 10^{-7}$, $t(26) = 6.4$; drugs *vs.* 4F4PP $P = 0.35$, $t(26) = 0.95$). Application of 5-HT2A receptor agonist TCB2 (10 μM) increased the firing frequency (**o**, Wilcoxon matched pairs test $P = 0.0014$, $Z = 3.2$). All data are presented as mean ± s.e.m.

Europe PMC Funders Author Manuscripts

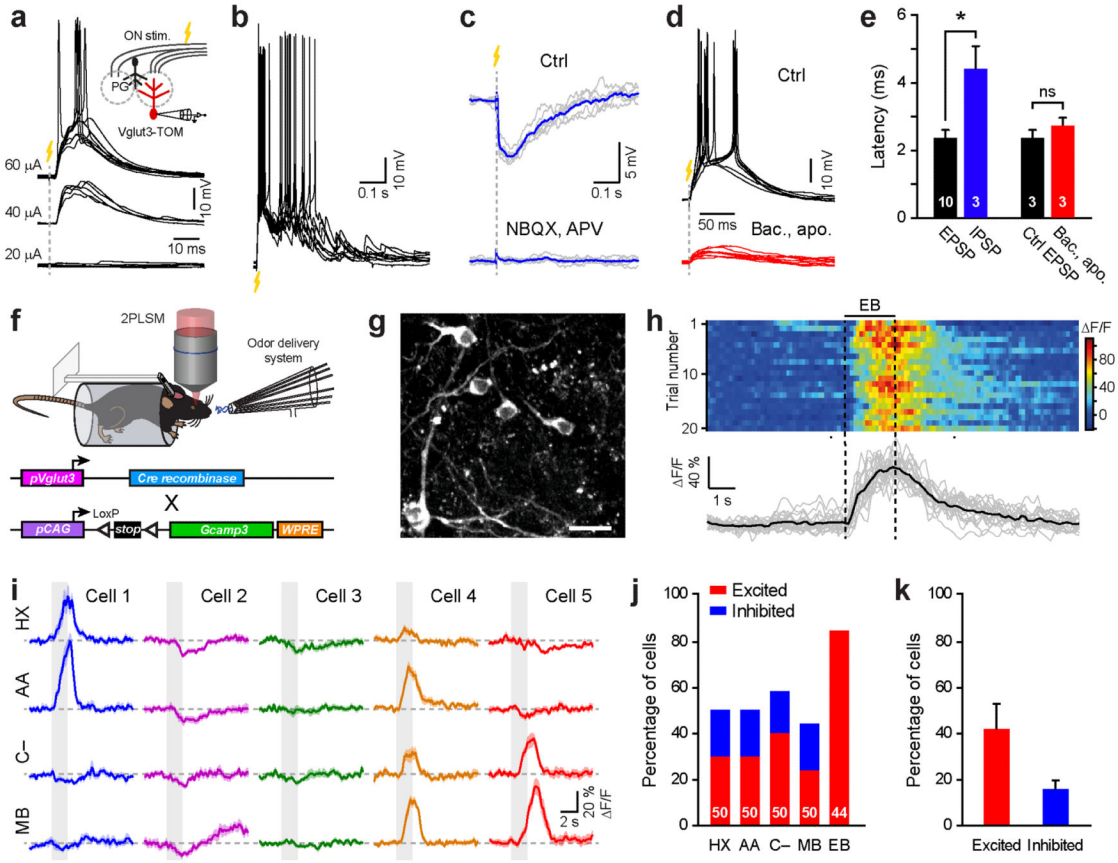

Figure 7. Vglut3 neuron responses to sensory inputs stimulation

(**a**) Synaptic responses evoked by increasing intensities of olfactory nerve (ON) stimulation (20 µA, 40 µA and 60 µA) in a VGLUT3 neuron. Yellow lightning and dotted line indicate ON stimulation (similar convention in subsequent panels). (**b**) Higher stimulation intensities evoked bursts of APs and long-lasting depolarization. (**c**) Superimposed traces of ON-evoked IPSPs in another Vglut3-TOM·cell recorded in control and during application of 10 µM NBQX and 100 µM dl-APV. Average traces are shown in blue. (**d**) ON-evoked response in ACSF (Ctrl) and in presence of 10 µM (RS)-baclofen and 30 µM apomorphine in a TOM^+ neuron. (**e**) Histogram summarizing the latencies of evoked EPSPs and IPSPs for different cells and for different conditions (EPSP vs. IPSP: Mann-Whitney U test: $n = 10$, $Z = -2.28$, $^*P = 0.022$; Ctrl vs. Bac/apo: Wilcoxon matched pairs test: $n = 3$, $Z = 1.6$, $P = 0.11$). White numbers indicate the number of recorded cells. (**f**) Schema of the experimental procedure: odorant-evoked Ca^{2+} responses were recorded from the somata of Vglut3-GCaMP3 neurons in awake head-restrained mice using a two-photon laser-scanning microscope (2PLSM). (**g**) Z-stack projection of $GCaMP3^+$ neurons imaged in an awake mouse (scale bar: 20 µm). (**h**) Ca^{2+} transients evoked by several repetitions of ethyl butyrate (EB) application imaged in a $GCaMP3^+$ neuron. Gray lines: twenty individual trials. Black line: average response. (**i**) Examples of the averaged Ca^{2+} signals (shaded areas represent s.e.m.) evoked by different odorants in several $GCaMP3^+$ neurons. Methyl benzoate (MB), carvone–(C−), amyl acetate (AA), and 3-Hexanone (HX). Gray boxes indicate odor application. Cells 1 to 3 and cells 4-5 are representative examples taken from two animals, respectively. (**j**) Fraction of cells

Europe PMC Funders Author Manuscripts

excited and inhibited by different odorants. White numbers indicate the number of imaged cells (*n* =6 mice). (**k**) Average fraction of cells excited or inhibited by different odorants. All data are presented as mean ± s.e.m.

Europe PMC Funders Author Manuscripts

Europe PMC Funders Author Manuscripts

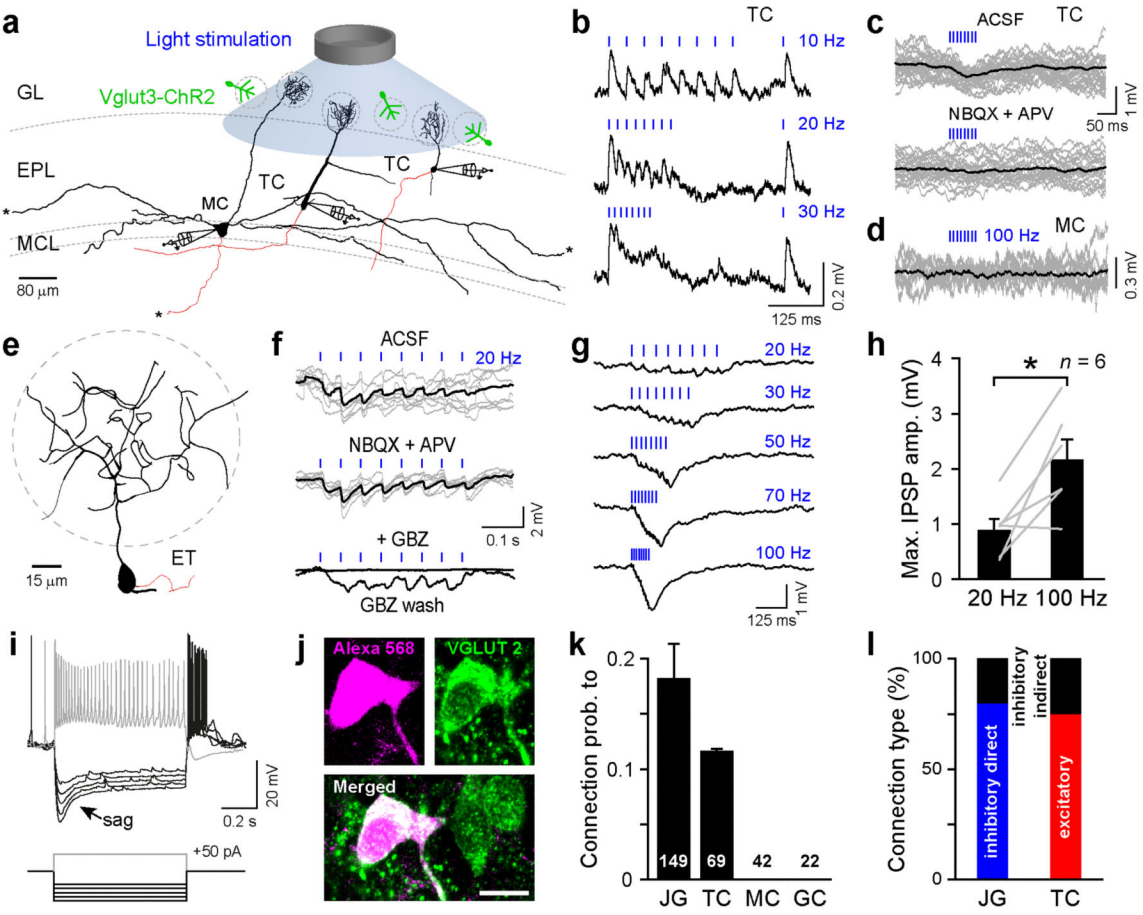

Figure 8. VGLUT3 neurons differentially control output neurons of the OB

(**a**) Schema illustrating the experimental procedure. Montage of different cell types recorded and reconstructed from different slices. MC: mitral cell, TC: tufted cell. Axons appear in red. For simplicity, axons and dendrites were truncated in the illustration (black stars). (**b**) Light-evoked EPSPs recorded from a TC at different stimulation frequencies. Each trace represents the average of 20 repetitions. (**c**) Single traces (*gray*) and average trace (*black*) showing light-evoked IPSPs recorded from TC in different pharmacological conditions. (**d**) Single traces (*gray*) and average trace (*black*) showing the absence of light-evoked PSP on a representative MC. (**e-f**) IPSPs evoked by light stimulation in different pharmacological conditions recorded from the VGLUT3 negative external tufted cell reconstructed in (**e**). Axon appears in red. (**g**) Light-evoked IPSPs recorded from a different VGLUT3$^-$ ET cell in response to light trains at different frequencies. (**h**) Histogram showing maximum IPSP amplitude evoked by 20 and 100 Hz light stimulation in VGLUT3$^-$ ET cell (Wilcoxon matched pairs test **P* = 0.046, *Z* = 1.99). Data are presented as mean ± s.e.m. (**i**) Typical response of a VGLUT3$^-$ ET cell to injection of negative or positive pulses of current. Note the presence of sag and rebound spiking following hyperpolarization. (**j**) VGLUT3$^-$ ET cell are immunostained for VGLUT2 (scale bar: 10 µm). (**k**) Graph summarizing the probability of connection made by VGLUT3$^+$ neurons onto different cell types of the OB. GC: granule cell. Numbers of recorded cells are indicated on the bars. Error bars are computed assuming binomial distribution (i.e. s.e.m. = $\sqrt{[f(1-f)/n]}$, where *f* is the fraction of modulated cells and *n*

is the total number of recorded neurons). (**I**) Graph summarizing the different types of connections recorded from JG cells and TC.

Europe PMC Funders Author Manuscripts

Europe PMC Funders Author Manuscripts

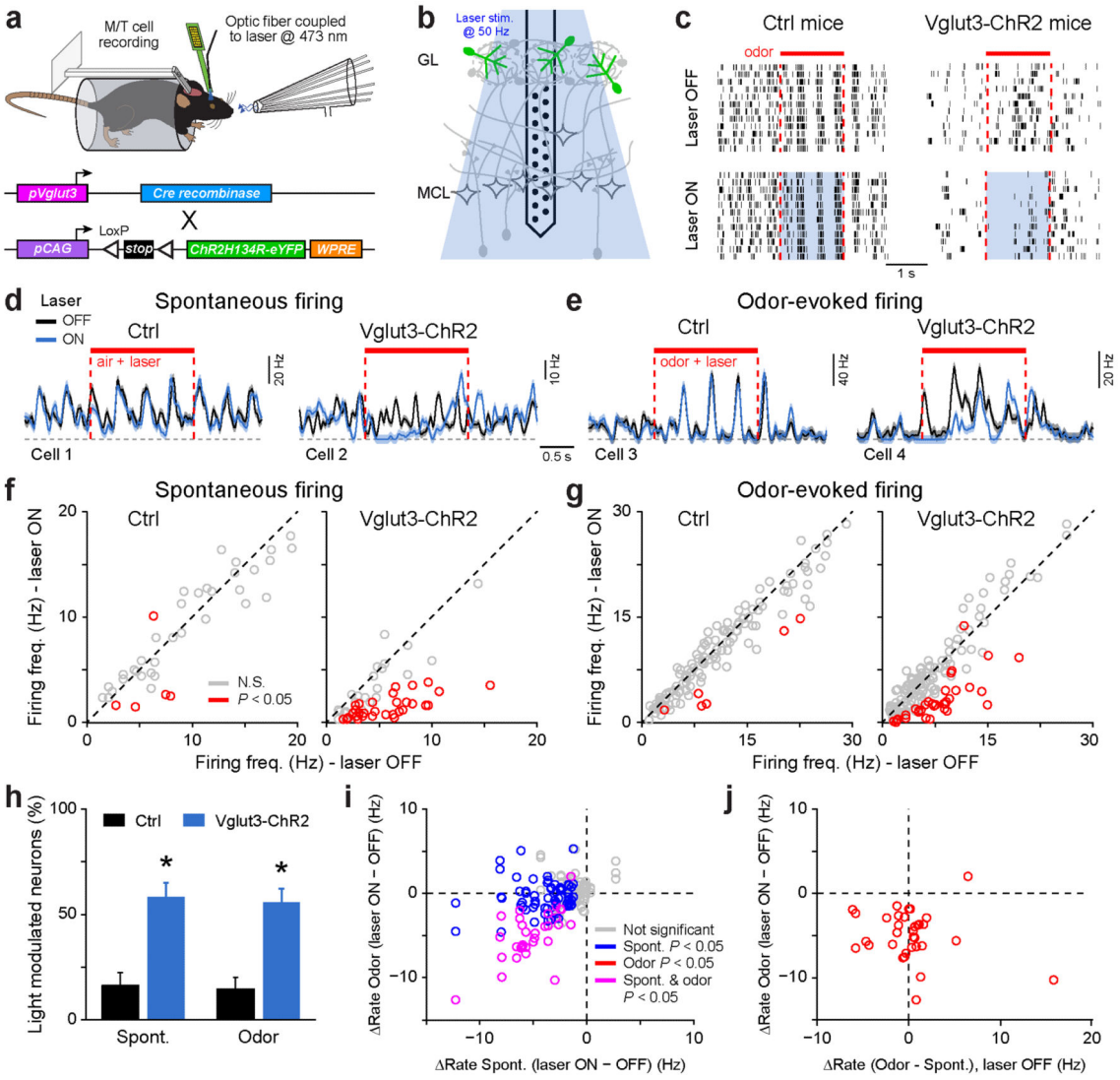

Figure 9. VGLUT3 neurons stimulation suppresses the firing of OB output neurons *in vivo*

(**a-b**) Schema illustrating the experimental procedure. Optrodes are placed in the OB to simultaneously record M/T cells and stimulate VGLUT3 neurons expressing channelrhodoposin-2 with a laser-coupled optic fiber. (**c**) Examples of raster plots for M/T single units recorded in control and in Vglut3-ChR2 mice. Odor-evoked firing is selectively suppressed by photostimulation (laser ON) in Vglut3-ChR2 mice. (**d-e**) Peristimulus time histrograms (PSTHs) in control (black traces) and during photostimulation (blue traces) show a selective suppression of both spontaneous (**d**) and odor-evoked (**e**) firing in M/T cells recorded in Vglut3-ChR2 mice. Shaded areas represent s.e.m. (**f-g**) Summary plots showing the effect of photostimulation on spontaneous (**f**; n = 42 and 55 single units for ctrl and Vglut3-ChR2 mice, respectively) and odor-evoked (**g**; n = 126 and 165 cell/odor pairs for ctrl and Vglut3-ChR2, respectively) firing. Red circles represent cells displaying a significant rate change evoked by photostimulation (paired t-test $P < 0.05$ plus Bonferoni correction). (**h**) Fraction of cells significantly modulated by photostimulation (n = 42 and 55 M/T units for ctrl and Vglut3-ChR2, respectively). Error bars are computed assuming

binomial distribution (i.e. s.e.m. = $\sqrt{[f(1-f)/n]}$, where f is the fraction of modulated cells and n is the total number of recorded neurons). The fraction of cells modulated by photostimulation is significantly higher in Vglut3-ChR2 mice (χ^2 test $^*P = 0.0002$). (**i**) Scatter plot showing the effect of photostimulation on both spontaneous and odor-evoked firing for all recorded neurons in Vglut3-ChR2 mice. Each circle represents a cell/odor pair. (**j**) Scatter plot shows neurons recorded in Vglut3-ChR2 mice and significantly changing their odor-evoked firing after photostimulation. Each circle represents a cell/odor pair. Stimulation suppresses odor-evoked firing independently of whether odor-evoked response in absence of photostimulation where excitatory or inhibitory.

Europe PMC Funders Author Manuscripts

Europe PMC Funders Author Manuscripts

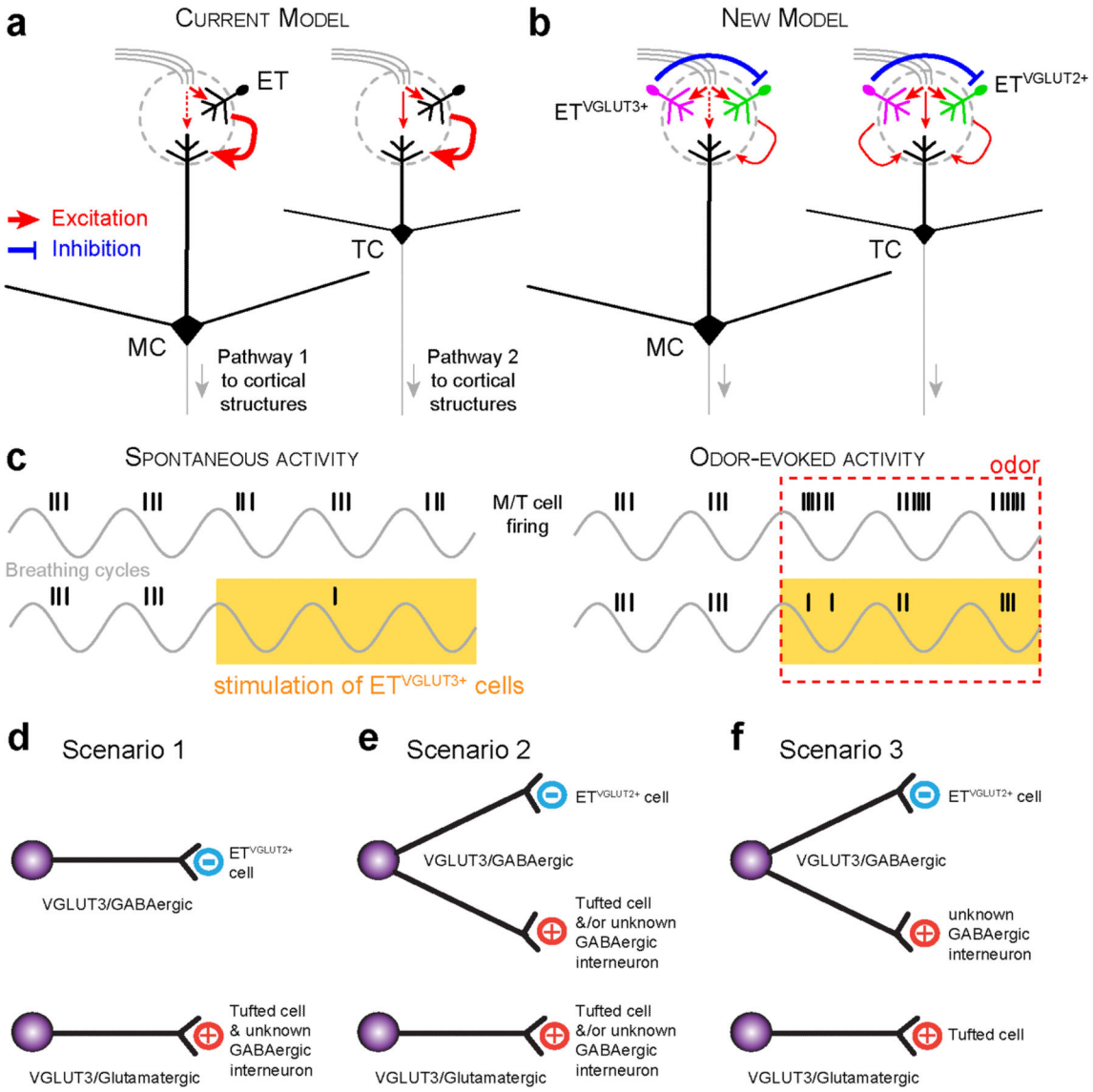

Figure 10. Schema summarizing the findings

(**a**) Current model based on several studies[3-6]. Upon nerve stimulation, mitral cells (MCs) receive weak inputs (dotted arrow) from OSNs and they are mainly stimulated through a multistep excitation mediated by external tufted (ET) cells (thick arrow). Similar mechanism may recruit tufted cells (TCs) though they receive stronger nerve inputs (plain arrow). For clarity, axons from ET cells have been omitted. (**b**) In the new model, multistep excitation of output neurons would be mediated by $ET^{VGLUT2+/VGLUT3-}$ cells. In addition, we identify a novel population of $ET^{VGLUT3+}$ cells which both excites tufted cells and inhibits $ET^{VGLUT2+}$ neurons. When stimulated, $VGLUT3^{+}/VGAT^{+}$ neurons should directly inhibit $ET^{VGLUT2+}$ and reduce the feedforward excitation on M/T cells. It follows that output neurons firing would be reduced. (**c**) Consistent with the new model, stimulation of $VGLUT3^{+}$ neurons *in vivo* suppresses both spontaneous and odor-evoked firing of bulbar output neurons. Possible connectivity patterns involving different VGLUT3 neuron subpopulations. (**d**) In a first scenario, VGLUT3/GABAergic neurons could specifically

contact $ET^{VGLUT2+/VGLUT3-}$ cells while VGLUT3/glutamatergic neurons target tufted cells. (**e**) In a second scenario, VGLUT3/GABAergic neurons would release both neurotransmitters at different terminals. The same VGLUT3/GABAergic neuron would inhibit $ET^{VGLUT2+}$ and excite TC and/or unknown GABAergic interneurons. (**f**) In a third scenario, VGLUT3/GABAergic neurons would release both GABA on $ET^{VGLUT2+}$ and glutamate on GABAergic interneurons that we have not yet identified. In contrast VGLUT3/glutamatergic neurons would still target tufted cells. In this scenario the VGLUT3/GABAergic population would contribute to strongly inhibit output neurons through a complex intra-glomerular inhibition (i.e. reduced excitation of output neurons due to inhibition of $ET^{VGLUT2+}$ combined with a feedforward inhibition mediated by excitation of undetermined GABAergic neurons).

Europe PMC Funders Author Manuscripts